HHS Public Access

Author manuscript

Neurobiol Dis. Author manuscript; available in PMC 2023 November 28.

Published in final edited form as:

Neurobiol Dis. 2023 February ; 177: 105998. doi:10.1016/j.nbd.2023.105998.

P-Rex1 is a novel substrate of the E3 ubiquitin ligase Malin associated with Lafora disease

L. Kumarasinghe[1], **M.A. Garcia-Gimeno**[2], **J. Ramirez**[3], **U. Mayor**[3,4], **JL. Zugaza**[4,5,6], **P Sanz**[1,*]

[1]Instituto de Biomedicina de Valencia. IBV-CSIC. 46010-Valencia. Spain, and Centro de Investigación Biomédica en Red de Enfermedades Raras (CIBERER)-ISCIII. 28029-Madrid. Spain.

[2]Department of Biotechnology. Escuela Técnica Superior de Ingeniería Agronómica y del Medio Natural (ETSIAMN). Universitat Politécnica de València. 46022-Valencia. Spain.

[3]Department of Biochemistry and Molecular Biology. Faculty of Science and Technology. UPV/EHU. Leioa. Bizkaia. Spain.

[4]Ikerbasque. Basque Foundation for Science. Plaza Euskadi. 48009 Bilbao. Spain

[5]Achucarro Basque Center for Neuroscience. Scientific Park UPV/EHU. 48940 Leioa. Bizkaia. Spain.

[6]Department of Genetics. Physical Anthropology and Animal Physiology. Faculty of Science and Technology. UPV/EHU. 48940 Leioa. Bizkaia. Spain.

Abstract

Laforin and Malin are two proteins that are encoded by the genes *EPM2A* and *EPM2B*, respectively. Laforin is a glucan phosphatase and Malin is an E3-ubiquitin ligase, and these two proteins function as a complex. Mutations occurring at the level of one of the two genes lead to the accumulation of an aberrant form of glycogen meant to cluster in polyglucosans that go under the name of Lafora bodies. Individuals affected by the appearance of these polyglucosans, especially at the cerebral level, experience progressive neurodegeneration and several episodes of epilepsy leading to the manifestation of a fatal form of a rare disease called Lafora disease (LD), for which, to date, no treatment is available. Despite the different dysfunctions described for this disease, many molecular aspects still demand elucidation. An effective way to unknot some of the nodes that prevent the achievement of better knowledge of LD is to focus on the substrates that are ubiquitinated by the E3-ubiquitin ligase Malin. Some substrates have already been provided by previous studies based on protein-protein interaction techniques and have been associated with some alterations that mark the disease. In this work, we have used an unbiased alternative approach based on the activity of Malin as an E3-ubiquitin ligase. We report the discovery of novel bonafide substrates of Malin and have characterized one of them more deeply, namely PIP_3-dependent Rac exchanger 1 (P-Rex1). The analysis conducted upon this substrate sets the

[*]**Corresponding author**: Dr. Pascual Sanz. Instituto de Biomedicina de Valencia. Consejo Superior de Investigaciones Científicas. Jaime Roig 11. 46010-Valencia. Spain. Tel. +34-963391779. FAX. +34-963690800. sanz@ibv.csic.es.

CONFLICT OF INTEREST STATEMENT

All the authors declare they have no conflict of interest.

genesis of the delineation of a molecular pathway that leads to altered glucose uptake, which could be one of the origin of the accumulation of the polyglucosans present in the disease.

Keywords

Lafora disease; ubiquitination; quantitative proteomics; bioUb; P-Rex1; Rac1; Malin

INTRODUCTION

Lafora disease (LD, OMIM#254780) is a rare and fatal form of progressive myoclonus epilepsy. The hallmark of the disease is the accumulation of insoluble and abnormal forms of glycogen depositing especially in the brain and peripheral tissues (Lafora and Glueck, 1911), (Sakai et al., 1970). These glycogen-like inclusions, also known as polyglucosans, were first described by the Spanish Neurologist Dr. Gonzalo Rodriguez Lafora (Lafora and Glueck, 1911), and named after him as Lafora bodies (LBs). Affected individuals show the first symptoms during adolescence. In the early stages of the disease patients are marked by a change in behavior, depression, and dysarthria until they reach a worsening condition characterized by myoclonic episodes, seizures, and rapid progressive neurodegeneration. From the onset of the first symptoms, patients have a median disease duration of 11 years (Turnbull et al., 2012), (Turnbull et al., 2016), (Pondrelli et al., 2021). To date, there is no effective therapy that can solve the disease but there are palliative treatments, such as the use of anti-seizure medications, to which patients, after some time, develop resistance (Garcia-Gimeno et al., 2018). Intending to develop a new therapy, different studies have focused on the role of glycogen synthase, the enzyme involved in the synthesis of glycogen. Different groups have shown how a reduction in the synthesis of glycogen can decrease the production of polyglucosans in Lafora disease models (Pederson et al., 2013), (Turnbull et al., 2011), (Turnbull et al., 2014). The obtained results prompted the researchers to develop new strategies such as the use of antisense oligonucleotides that can decrease the expression of glycogen synthase (Ahonen et al., 2021) or the use of new compounds that can directly digest the Lafora bodies leading to their reduction (Brewer and Gentry, 2019).

LD is an autosomal recessive disease and, with a prevalence of fewer than 4 patients out of 1,000,000 individuals, it is classified as a rare neurological disorder (Turnbull et al., 2016). Concerning its features, it belongs to a group of diseases known as Progressive Myoclonus Epilepsies (PMEs) (Kalviainen, 2015). In ≈44% of the cases LD is caused by mutations that fall on the *EPM2A* gene encoding the glucan phosphatase Laforin (Roma-Mateo et al., 2011), (Minassian et al., 1998), (Serratosa et al., 1999), (Pondrelli et al., 2021), while in the ≈56% of the cases mutations occur on the *EPM2B/NHLRC1* gene encoding the RING-type E3-ubiquitin ligase Malin, (Turnbull et al., 2016), (Chan et al., 2003), (Pondrelli et al., 2021). The two proteins, Laforin and Malin, work together as a regulated complex, and mutations that happen on either of the two genes break the harmonious system. Presumably, their function as a complex explains why patients reporting mutations on either *EPM2A* or *EPM2B* show similar pathological phenotypes, and why mutations affecting the interaction between the two proteins lead also to disease (Garcia-Gimeno et al., 2018), (Roma-Mateo et al., 2011), (Gentry et al., 2005), (Solaz-Fuster et al., 2008), (Rubio-Villena et al., 2013).

LD can be, in part, considered a disease related to the ubiquitin system (Garcia-Gimeno et al., 2018). Malin, as an E3-ubiquitin ligase and due to its structure, is defined as a Tripartite Motif (TRIM)-like protein (Kumarasinghe et al., 2021). TRIM proteins are defined as a subfamily of the RING-type E3 ubiquitin ligase family (Reymond et al., 2001), (Meroni and Desagher, 2022), and are involved in the last step of the ubiquitination process where substrates are recognized, ubiquitinated, and directed towards different cellular fates depending on the type of mono- or polyubiquitin chain they carry (Swatek and Komander, 2016), (Mallette and Richard, 2012), (Hatakeyama, 2017), (Meroni, 2020). The ubiquitination of specific substrates by Malin requires its interaction with E2-conjugating enzymes such as E2 UBE2N, which promote K63-linked polyubiquitination (Sanchez-Martin et al., 2015). To date, several substrates of Malin have been identified (Solaz-Fuster et al., 2008), (Rubio-Villena et al., 2013), (Sanchez-Martin et al., 2015), (Sharma et al., 2012), (Moreno et al., 2010), (Viana et al., 2015), (Sanchez-Martin et al., 2020), (Perez-Jimenez et al., 2021), and their discovery helped delineating some of the pathophysiological features of the disease defined so far: accumulation of polyglucosans (Solaz-Fuster et al., 2008), (Rubio-Villena et al., 2013), (Cheng et al., 2007); increase in glucose uptake (Singh et al., 2012); impairment in the degradation processes at the level of the proteasome and autophagy (Sanchez-Martin et al., 2020), (Aguado et al., 2010), (Puri and Ganesh, 2012); alteration of glutamatergic transmission (Perez-Jimenez et al., 2021), (Munoz-Ballester et al., 2016); mitochondrial dysfunction (Roma-Mateo et al., 2015a), (Roma-Mateo et al., 2015b), (Lahuerta et al., 2018); and neuroinflammation (Lopez-Gonzalez et al., 2017), (Lahuerta et al., 2020). However, most of the molecular mechanisms that underlie these features require in-depth study to shed light on the different obscure points of the disease. Certainly, the search for new substrates could be useful for different purposes: to better understand the various pathophysiological alterations described so far, the discovery of new unknown dysfunctions of the disease, and the development of new therapeutic strategies.

As most of the possible substrates of Malin have been identified only by using protein-protein interaction techniques (Co-Immunoprecipitation, yeast two-hybrid, etc.) (Garcia-Gimeno et al., 2018), in this work, we have used an unbiased alternative strategy based on the activity of Malin as an E3-ubiquitin ligase. By using a ^{bio}Ub strategy (Martinez et al., 2017), (Ramirez et al., 2018), we describe a set of proteins whose ubiquitination is increased in cells expressing Malin wild type in comparison to cells expressing an inactive form of Malin (P69A) and characterized one of these novel substrates, namely PIP3-dependent Rac exchanger 1 (P-Rex1).

MATERIALS AND METHODS

Mammalian cell culture

Human embryonic kidney cells (HEK293) (HPA Culture Collection#851820602) were used for transfection experiments. Cells were grown in Dulbecco's modified Eagle medium (Lonza. Barcelona. Spain), supplemented with 10% inactivated fetal bovine serum (FBS) (Invitrogen. Madrid. Spain), 1% L-glutamine, 100 units/ml penicillin, and 100 μg/ml streptomycin in a humidified atmosphere at 37°C and 5% (vol/vol) of CO_2.

Preparation of mouse primary astrocytes

This study was carried out in strict accordance with the recommendations in the Guide for the Care and Use of Laboratory Animals of the Consejo Superior de Investigaciones Cientificas (CSIC, Spain) and approved by the Consellería de Agricultura, Medio Ambiente, Cambio Climático y Desarrollo Rural from the Generalitat Valenciana. All mouse procedures were approved by the animal committee of the Instituto de Biomedicina de Valencia-CSIC [Permit Number: IBV-51, 2019/VSC/PEA/0271]. All efforts were made to minimize animal suffering. Mouse primary astrocytes from control and *Epm2b*−/− mice (Lahuerta et al., 2020) were obtained from P0 to P1 mice. Cortices, including the hippocampus, were dissected, the meninges were removed, and the tissues were homogenized using the Neural Tissue Dissociation kit and the GentleMACS dissociator from Mylteny Biotec (Madrid. Spain). Once obtained, microglia contamination was removed using CD11b Microbeads in a magnetic field (Mylteny Biotec. Madrid. Spain). Cells were grown in Dulbecco's modified Eagle medium (Lonza. Barcelona. Spain) containing 20% of inactivated FBS, supplemented with 1% L-glutamine, 7.5 mM glucose, 100 units/ml penicillin, and 100 μg/ml streptomycin, in a humidified atmosphere at 37°C with 5% of CO_2. After 48 h, FBS was reduced to 10% and cultures were shacked at 200 rpm for 4h to remove residual oligodendrocytes and microglial cells. For the following 10 days, 0.25 mM dibutyryl-cAMP (dbcAMP) (D0627, Sigma-Aldrich) was added to the cultures to favor astrocytes' maturation. At the end of the maturation process, primary astrocytes were grown for a further 48 h in the absence of dbcAMP to avoid any undesired effect deriving from the compound (Hertz et al., 1998), (Muller et al., 2014), (Magistretti et al., 1983).

Plasmid constructs

The following plasmids were described in reference (Sanchez-Martin et al., 2015): pFLAG-Laforin, pECFP-Laforin, pEGFP-Malin, and pFLAG-Malin. Plasmid pFLAG-Malin P69A was described in reference (Couarch et al., 2011); Dr. Atanasio Pandiella (CIC-Salamanca) kindly provided plasmid Myc-P-Rex1; plasmid pCMV-6xHisUbiq was generously provided by Dr. Manuel Rodríguez (Proteomics Unit. CIC-bioGUNE, Bizkaia, Spain) and plasmids pCMV-6xHis-Ubiq-K48R and pCMV-6xHis-Ubiq-K63R were a generous gift of Dr. Ch. Blattner (Institute of Toxicology and Genetics. Karlsruhe Institute of Technology, Karlsruhe, Germany). Plasmid pCEFL-AU5-Rac1 was provided by Dr. Jose Luis Zugaza (Achucarro Basque Center for Neuroscience. Leioa, Bizkaia, Spain). The GST fusion protein containing the Rac1 binding domain of PAK1 (GST-RBD-PAK1) was obtained as described in (Arrizabalaga et al., 2012). pCAG-(bioUb)x6-BirA plasmid was described in (Ramirez et al., 2021b).

Biotin pulldown

For the analysis of differentially ubiquitinated Malin substrates, we applied the ^{bio}Ub strategy described in previous reports (Martinez et al., 2017), (Ramirez et al., 2018), (Lectez et al., 2014), (Ramirez et al., 2015), (Pirone et al., 2017), (Elu et al., 2019), (Ramirez et al., 2021a). Briefly, 13.5×10^6 cells were seeded in three independent 150 mm dishes for each experimental condition (WT and Malin-P69A). After 48 h, cells were transfected with either FLAG-Malin or FLAG-Malin P69A and the pCAG-(bioUb)x6-BirA plasmid

(Franco et al., 2011), (Elu et al., 2020), a construct expressing a precursor polypeptide composed of six biotinylatable versions of ubiquitin, conjugated to BirA, the *E. coli* biotin ligase enzyme, using lipofectamine 3000 reagent (Invitrogen. Madrid, Spain), according to the manufacturer's instructions, and supplemented with 50 μM biotin solution. The ^{bio}Ub construct (^{bio}Ub-BirA) gets digested in the cells by the endogenous deubiquitinating enzymes (DUBs) leading to the release of BirA and bio-Ub. Then, BirA recognizes the short specific N-terminal sequence of each modified ubiquitin and biotinylates it, generating biotin-tagged-ubiquitins. This reaction is executed very efficiently with minor off-targets. The biotin-tagged-ubiquitins are then incorporated into the cascade of the ubiquitination process to modify the corresponding proteins (Fig. 1A). The next day, cells were harvested and lysed with 2.5 ml of a solution containing 8 M urea, 1 % SDS, 50 mM N-ethylmaleimide (Sigma-Aldrich), and a complete protease inhibitor cocktail (Roche Diagnostics, Barcelona, Spain). Lysates were then passed through a 20G needle 10 times and applied to a PD10 desalting column (GE Healthcare. Barcelona, Spain), previously equilibrated with 25 ml of 3 M urea, 1 M NaCl, 0.25% SDS, and 50 mM N-ethylmaleimide. Recovered eluates were incubated with 150 μl of NeutrAvidin agarose beads suspension (Thermo Fisher Scientific, Waltham, MA. USA), and gentle rolling for 40 min at room temperature and 2 h at 4°C. Afterward, beads were washed with the following solutions: twice with 8 M urea and 0.25 % SDS, thrice with 6 M guanidine-HCl, once with 6.4 M urea, 1 M NaCl and 0.2 % SDS, thrice with 4 M urea, 1 M NaCl, 10 % isopropanol, 10 % ethanol, and 0.2 % SDS, once again with 8 M urea and 0.25 % SDS, once with 8 M urea and 1 % SDS, and thrice with 2 % SDS. All the solutions were prepared in PBS. Ubiquitinated material was then eluted with 80 μl of elution buffer (250 mM Tris-HCl, pH 7.5, 40% glycerol, 4% SDS, 0.2% bromophenol blue, and 100 mM DTT) boiling them at 95°C for 5 min. Samples were subjected to final centrifugation at 16.000 × *g* in a Vivaclear Mini 0.8 μm PES-micro-centrifuge unit (Sartorius. Madrid, Spain) to discard the NeutrAvidin resin used. A similar amount of total ubiquitinated material was recovered in cells transfected with FLAG-Malin or FLAG-Malin P69A (Fig. 1B).

Liquid chromatography with tandem mass spectrometry (LC-MS/MS)

Eluates from biotin pull-down assays were resolved by SDS-PAGE using 4–12% Bolt Bis-Tris Plus pre-cast gels (Invitrogen. Carlsbad. CA. USA) and visualized with GelCode Blue Stain reagent following manufacturer's instructions (Thermo Fisher Scientific, Waltham, MA. USA). After the exclusion of avidin monomers and dimers, each lane was cut into four slices and subjected to in-gel digestion as described previously (Ramirez et al., 2021b), (Osinalde et al., 2015).

Mass spectrometric analyses were performed on an EASY-nLC 1200 liquid chromatography system interfaced via a nanospray flex ion source with Q Exactive HF-X (Thermo Fisher Scientific. Waltham. MA. USA). Peptides were loaded onto an Acclaim PepMap100 pre-column (75 mm × 2 cm. Thermo Fisher Scientific. Waltham. MA. USA) connected to an Acclaim PepMap RSLC (50 mm × 25 cm Thermo Fisher Scientific. Waltham. MA. USA) analytical column. Peptides were eluted from the columns using a two-step gradient of 2.4 to 24% (90 min) and 24 to 32% (2 min) acetonitrile in 0.1% of formic acid at a flow rate of 300 nL min^{-1} over 92 min. The mass spectrometers were operated in positive ion mode.

Full MS scans were acquired from m/z 375 to 1850 with a resolution of 60.000 at m/z 200. The 10 most intense ions were fragmented by high-energy collision dissociation (HCD) with a normalized collision energy of 28 and MS/MS spectra were recorded with a resolution of 15.000 at m/z 200. The maximum injection time was 50 ms for the survey and 100 ms for MS/MS scans, whereas AGC target values of 3×10^6 and 1×10^5 were used for the survey and MS/MS scans, respectively. To avoid repeat sequencing of peptides, dynamic exclusion was applied for 20 s. Singly charged ions or ions with unassigned charge states were also excluded from MS/MS. Data were acquired using Xcalibur software (Thermo Fisher Scientific. Waltham. MA. USA).

Data Processing and Bioinformatics Analysis

Acquired raw data files were processed with the MaxQuant (Cox and Mann, 2008) software (versions 1.5.3.17 and 1.6.0.16) using the internal search engine Andromeda and searched against the UniProtKB database restricted to Homo sapiens (20,187 entries), as described in (Ramirez et al., 2021b). Spectra originated from the different slices corresponding to the same biological sample were combined. Carbamidomethylation (C) was set as fixed modification, whereas Met oxidation, protein N-terminal acetylation, and Lys GlyGly (not C-term) were defined as variable modifications. Mass tolerance was set to 8 and 20 ppm at the MS and MS/MS level, respectively; except in the analysis of the TOF data for which the values of 0.006 Da and 40 ppm were used, respectively. Enzyme specificity was set to trypsin, allowing for cleavage N-terminal to Pro and between Asp and Pro with a maximum of two missed cleavages. Match between runs option was enabled with 1.5 min match time window and 20 min alignment window to match identification across samples. The minimum peptide length was set to seven amino acids. The false discovery rate for peptides and proteins was set to 1%. Normalized spectral protein label-free quantification (LFQ) intensities were calculated using the MaxLFQ algorithm. To further clarify, the following default parameters from MaxQuant were used: Decoy mode, revert; PSM FDR, 0.01; Protein FDR, 0.01; Site FDR, 0.01. MaxQuant output data was then analyzed with Perseus software (version 1.6.0.7) (Tyanova et al., 2016), and statistically significant differences in protein abundance were determined by a two-tailed Student’s t-test.

Analysis of protein ubiquitination

The method described in (Kaiser and Tagwerker, 2005) was used to study the ubiquitination of P-Rex1. For this purpose, HEK293 cells were transfected with the plasmids indicated in each experiment using X-treme GENE HP transfection reagent according to the manufacturer’s protocol (Roche Diagnostics, Barcelona, Spain). After 24 h of transfection, cells were lysed using a 25-gauge needle in buffer A (6 M guanidinium-HCl, 0.1 M sodium phosphate, 0.1 M Tris-HCl pH 8.0) to inhibit the action of endogenous deubiquitinases. Protein extracts were clarified after centrifugation (12.000 × g 15 min) and protein concentration was measured through the Bradford technique. 1.5 mg of protein were incubated with 150 μl of a TALON cobalt resin (Clontech. Barcelona. Spain) equilibrated in buffer B containing 10 mM imidazole, 6 M guanidinium-HCl, 0.1 M sodium phosphate, 0.1 M Tris-HCl pH 8.0. To purify His-tagged proteins, incubation was carried out for 2 h at room temperature on a rocking platform. Then, the resin was washed with 1 mL of buffer B and four times with buffer C (buffer B, but with 8 M urea instead of 6 M guanidinium-HCl).

Bound proteins were boiled at 95°C for 5 min in 50 μl of 2×Laemmli's sample buffer and analyzed by Western blotting using the appropriate antibodies. To determine the topology of the ubiquitin chains, when indicated, plasmids pCMV-6xHis-Ubiq-K48R and pCMV-6xHis-Ubiq-K63R were used in the assay instead of pCMV-6xHis-Ubiq wild type.

GFP-trap analysis of protein-protein interactions

HEK293 cells were transfected with specific constructs of Laforin, Malin, and the protein of interest. Cells were washed twice with cold phosphate-buffered saline (PBS) and scraped on ice in lysis buffer [10 mM Tris–HCl pH 7.5, 150 mM NaCl, 0.5 mM EDTA, 0.5% (v/v) Nonidet P-40, complete protease inhibitor cocktail (Roche Diagnostics. Barcelona. Spain), 1 mM PMSF, 2.5 mM NaF, 0.5 mM $NaVO_4$, and 2.5 mM $Na_4P_2O_7$]. The lysates were collected in an Eppendorf tube and further lysis was performed using a 25-gauge needle. Cell lysates were then centrifuged at 13.000 × g for 10 min at 4°C. Supernatants (1.5 mg of total protein) were incubated with Chromotek GFP-trap beads (Chromotek, Planegg-Martinsried, Germany) for 1 h on a rocking platform at 4°C. Beads were washed two times with 1 mL of lysis buffer and one time with the lysis buffer containing 300 mM NaCl. Bound proteins were boiled at 95°C for 5 min in 30 μl of 2×Laemmli's sample buffer. The GFP- and CFP-fused proteins were pelleted and visualized by immunoblotting using specific antibodies. As a negative control, a construct expressing CFP or GFP proteins (plasmid pECFP-C1 and pEGFP-C1, respectively), was used to confirm the specificity of the interaction.

Western blot analyses

30 μg of total protein from the soluble fraction of cell lysates were analyzed by SDS-PAGE and proteins were transferred to PVDF membranes (Millipore. Madrid. Spain). Membranes were blocked with 5% (w/v) non-fat milk in Tris-buffered saline Tween20 buffer [TBS-T: 50 mM Tris-HCl pH 7.4, 150 mM NaCl, 0.1% (v/v) Tween20] for 1 hr at room temperature and incubated overnight at 4°C with the corresponding primary antibodies: rabbit anti-P-Rex1 (13168. Cell Signaling Technology, Barcelona, Spain), mouse anti-P-Rex1 (ab264535. Abcam, Madrid, Spain), mouse anti-Flag (F3165. Sigma-Aldrich, Madrid, Spain), rabbit anti-GFP (210-PS-1GFP. Inmunokontackt, Madrid, Spain), mouse anti-Rac1 (05–389. Millipore; Madrid, Spain), rabbit anti-GLUT1 (PA1–46152. Invitrogen. Madrid, Spain), goat anti-biotin-HRP-conjugated antibody (#7075. Cell Signaling Technology, Barcelona, Spain), and mouse anti-Na+/K+-ATPase (ab7671. Abcam. Madrid, Spain). Mouse anti-Gapdh (sc-32233. Santa Cruz Biotechnologies, Madrid, Spain), mouse anti-Tubulin (T6199. Sigma-Aldrich, Madrid, Spain), and rabbit anti-Actin (A2066. Sigma-Aldrich, Madrid, Spain), were used as loading controls. After washing, membranes were incubated with the corresponding HRP-conjugated secondary antibodies for 1 hr at room temperature. Signals were visualized using Lumi-Light Western Blotting Substrate (Roche Applied Science. Barcelona. Spain) or ECL Prime Western Blotting Detection Reagent (GE Healthcare. Barcelona. Spain), and analyzed by chemiluminescence using the FujiLAS400 (GE Healthcare, Barcelona, Spain) image reader. Quantification of the protein bands was carried out using the software Image Studio version 5.2 (LI-COR Biosciences, Germany).

Analysis of the Degradation Rate of P-Rex1

Mouse primary astrocytes from *Epm2b−/−* and control mice were treated with 70 μM cycloheximide (CHX; Sigma-Aldrich, Madrid, Spain) for the indicated times (from 0 to 24 h). Cells were lysed in cold cell lysis buffer [10 mM Tris pH 7.6, 150 mM NaCl, 1% Nonidet P-40, 10 mM $MgCl_2$, 1mM PMSF, complete protease inhibitor cocktail (Roche Diagnostics. Barcelona. Spain)], using a 25-gauge needle. Cell lysates were centrifuged at 13.500 rpm for 10 min at 4°C. 25 μg of cell extracts were analyzed by Western blotting using anti-P-Rex1 antibody. The same extracts were analyzed using anti-Tubulin antibody as a loading control.

Rac1 activation assay

Rac1 pulldown assay was performed using the GST-RBD-PAK1 fusion protein described above. 50 μg of this fusion protein were coupled to glutathione-sepharose beads for 1 hr at 4°C. HEK293 cells were transfected the day before with the plasmids indicated in the experiment. HEK293 cells were lysed in cold cell lysis buffer [10 mM Tris-HCl pH 7.6; 150 mM NaCl, 1% Nonidet P-40, 10 mM $MgCl_2$, 1mM PMSF, and complete protease inhibitor cocktail (Roche Diagnostics. Barcelona. Spain)] using a 25-gauge needle. Cell lysates were centrifuged at 13.500 rpm for 10 min at 4°C, and subsequently, 1 mg of protein extracts were incubated for 1 hr at 4°C with the preloaded glutathione-sepharose beads previously washed with lysis buffer three times to remove the excess of GST-RBD-PAK1 protein. Proteins bound to beads were washed three times, resuspended in 2×Laemmli's sample buffer, and analyzed by Western blotting using the appropriate antibodies.

Analysis of Glucose uptake

Glucose uptake was performed on mouse primary astrocytes control vs *Epm2b−/−* following the technical procedure described in the Glucose Uptake-Glo™ Assay manual (Promega #J1341. technical manual TM467). 30,000 cells/well were plated in 100 μL of culture medium in 96-well plates. Cells' maturation with dbcAMP was performed in the same support for 10 days. When indicated, cells were treated for 24 h with 2 μM 1.1-Dimethylbiguanide hydrochloride (Metformin) (D150959, Sigma-Aldrich, Madrid, Spain) before the assay. On the day of the assay, media was removed and cells were washed thoroughly with 1xPBS (BE17516Q, Lonza, Madrid, Spain) twice. 50 μL of 2-deoxyglucose (2-DG, final assay concentration of 1 mM) were added to each well for 10 min at room temperature. The assay was terminated by the addition of 25 μL of stop buffer, briefly mixed on an orbital shaker, and neutralized with 25 μL of neutralization buffer. Finally, 100 μL of 2DG6P Detection Reagent was added to each well, briefly mixed on an orbital shaker, and incubated for 1 hr at room temperature. Luminescence values were measured with a Tecan Spark microplate reader.

When indicated, glucose uptake was performed on cells in which the expression of P-Rex1 was silenced. For this purpose, 50,000 cells/well were plated in 200 μL of culture medium in 96-well plates. Silencing was performed after 10 days of maturation of the mouse primary astrocytes with dbcAMP following 24 h in culture media without dbcAMP. Cells were then transfected with 20 nM of Non Targeting pool siRNA (Cat#D-001810-10-05) or Smartpool Mouse P-Rex1 siRNAs (Cat#L-053658-00-0010) (Dharmacon/Horizon Discovery Ltd.

Madrid, Spain), using Lipofectamine Messenger Max Reagent (LMRNA008. Thermo Fisher Scientific; Madrid, Spain), for 48 hours before the glucose uptake.

Analysis of cell surface proteins by biotinylation

Cell surface biotinylation in mouse primary astrocytes was performed with the Pierce Cell Surface Protein Isolation kit (89881. Thermo Fisher Scientific, Madrid, Spain), according to the manufacturer's protocol. Briefly, 4×10^6 cells were grown on T75 Flasks. Cells' maturation with dbcAMP was performed in the same support for 10 days following 48 h in culture media without dbcAMP. On the day of the assay, cells were washed with PBS and incubated with EZ-LINK Sulfo-NHS-SS-biotin for 1 hr at 4°C followed by the addition of a quenching solution. Cells were lysed with the lysis buffer (500 μL) provided by the kit. An aliquot (100 μL) of the lysate was saved for Western blotting (total fraction). The biotinylated fraction was isolated with NeutrAvidin beads, eluted by the sample buffer (400 μL) containing DTT, and subjected to Western blot analysis. Appropriate antibodies were used to detect the proteins biotinylated at the level of the plasma membrane.

Statistical analysis

Results are shown as means +/− standard error of the mean (SEM) of at least three independent experiments. Differences between samples were analyzed by unpaired two-tailed Student's *t*-tests using Graph Pad Prism version 5.0 statistical software (La Jolla. CA. USA). P-values have been considered significant as *$p<0.05$, **$p<0.01$.

RESULTS

Identification of P-Rex1 as a novel substrate of Malin E3 Ubiquitin Ligase.

To search for possible novel substrates of Malin, we transfected HEK293 cells with plasmids expressing either FLAG-Malin-WT or FLAG-Malin-P69A. The mutation P69A is the most recurrent mutation in the *EPM2B* gene and leads to an inactive form of Malin (Couarch et al., 2011), (Riva et al., 2021). For the analysis of differentially ubiquitinated Malin substrates, we applied the ^{bio}Ub strategy described in Materials and Methods. Experiments were performed in three independent samples and subjected to liquid chromatography with tandem mass spectrometry (LC-MS/MS) analysis. By comparing their ubiquitomes, we identified the differentially ubiquitinated proteins present in cells expressing Malin-WT vs Malin-P69A.

Proteomic quantification can best be displayed on a volcano plot where abundance changes are provided on the X-axis, and the significance of these changes is displayed on the Y-axis (Fig. 2A). Endogenous carboxylases (ACACA and PC, which use biotin as a cofactor) appeared unchanged between both datasets, indicating that the amount of biological material was equivalent in both samples; ubiquitin itself also appeared unchanged between both datasets, as well as the avidin that is used for the pulldown, all these control proteins indicating that the experiment has worked correctly. Malin itself (NHLRC1) also appeared mostly unchanged between the two datasets (Figure 2A). Out of the 4465 proteins quantified, 88 proteins were found significantly enriched ($p<0.05$) by at least two-fold in cells expressing Malin-WT vs Malin-P69A. A DAVID analysis (https://david.ncifcrf.gov/) of

these proteins indicated that the biological processes where they were involved were mostly protein folding, response to heat shock, and regulation of mitochondrial function (Fig. 2B, top panel) and their molecular functions were heat shock proteins and ubiquitin ligases (Fig. 2B, bottom panel). A STRING analysis (https://string-db.org/) of the selected proteins indicated that most of them clustered in two groups, the heat shock protein (HSPs) group and the OXPHOS group, related to mitochondrial function (Fig. 2C). Both in Figure 2A and Table 1, we show the list of differentially ubiquitinated proteins with a fold change higher than 4.

Since P-Rex1 was the protein whose ubiquitination was most increased in cells expressing Malin-WT vs Malin-P69A (around 18-fold higher), we decided to characterize more deeply the consequences of its differential ubiquitination. We were also attracted by P-Rex1 because it is the first time that the activity of a GEF of Rac1 and Rac2 could be modulated by ubiquitination, in contrast to the most general modulation of GEF activity by phosphorylation (Crespo et al., 1997), (Llavero et al., 2015).

Validation of P-Rex1 as a substrate of Malin

According to Uniprot (https://www.uniprot.org/uniprot/Q8TCU6), P-Rex1 is a phosphatidylinositol-3,4,5-triphosphate dependent Rac exchanger factor (Rac-GEF). To consider P-Rex1 as a bonafide substrate of Malin, we validated its Malin-dependent ubiquitination by an alternative method, based on the expression in HEK293 cells of a modified form of ubiquitin tagged with 6xHis residues and the purification of ubiquitinated proteins by cobalt affinity chromatography (Kaiser and Tagwerker, 2005). In the pool of purified ubiquitinated proteins, the presence of P-Rex1 was assessed by using specific antibodies. Since the expression of endogenous P-Rex1 in HEK293 cells was very low, we expressed a myc-tagged-P-Rex1 version in combination with plasmids encoding Laforin and different forms of Malin. In cells co-transfected with the functional complex Laforin-Malin and myc-P-Rex1 (Fig 3A, lane 4), we observed higher ubiquitination of P-Rex1 in comparison to cells expressing only P-Rex1 (Fig. 3A, lane 1). In cells in which we co-transfected Laforin together with the inactive form of Malin (P69A), the rate of ubiquitination of the substrate was lower in comparison to cells expressing the wild type form of Malin (Fig. 3A, lane 5). On the other hand, in cells that were transfected only with the Malin-WT plasmid, the ubiquitination of P-Rex1 was also present (Fig 3A, lane 3), probably because cells contain enough endogenous levels of Laforin to allow the reaction, confirming the results obtained in the proteomic screening (see above). On the contrary, the expression of Laforin alone was not sufficient to enhance P-Rex1 ubiquitination (Fig. 3A, lane 2), over the basal level of ubiquitination of P-Rex1 obtained by the action of alternative endogenous E3-ligases (Fig. 3A, lane1). The lower panel in Fig. 3A shows the quantification of the ubiquitination signal. These results enable P-Rex1 to go from being a candidate to a bonafide substrate of Malin.

Moreover, we wanted to understand the type of polyubiquitin chains built on the substrate. Depending on the chain topology, substrate ubiquitination can signal many different cellular fates, among which, the most characterized is degradation by the proteasome, which is typical for substrates with K48 linked chains (Komander and Rape, 2012). For this purpose,

we used ubiquitin forms that carried K48R or K63R mutations. The use of these ubiquitin mutants would prevent the formation of K48-linked chains, in the case of the mutated form K48R, or of K63-linked chains, in the case of the K63R mutant. Figure 3B shows that the Laforin-Malin complex promotes the attachment of K63-linked ubiquitin chains. We can observe in the second lane of Fig. 3B an impairment of the ubiquitination of P-Rex1 in cells expressing the mutated ubiquitin form K63R, contrary to lane 1 where cells expressed K48R-ubiquitins (the lower panel shows the quantification of the ubiquitination signal). This result confirms that Malin favors the attachment of K63-linked polyubiquitin chains as demonstrated for other substrates in previous reports (Solaz-Fuster et al., 2008), (Rubio-Villena et al., 2013), (Sanchez-Martin et al., 2015), (Sharma et al., 2012), (Moreno et al., 2010), (Viana et al., 2015), (Sanchez-Martin et al., 2020), (Perez-Jimenez et al., 2021).

The Laforin-Malin complex interacts physically with P-Rex1

From a structural point of view, Malin is considered a TRIM-like protein. It is composed of an N-terminal RING domain, which confers catalytic activity, and a C-terminal domain represented by 6 NHL (present in NCL1, HT2A, and LIN-41 proteins) repeats (Gentry et al., 2005). However, unlike the typical TRIM proteins, Malin lacks the B-box and coiled-coil domains. In general, TRIM-E3 ligases are known to interact through the RING domain with the target substrate to confer specificity in the transfer of ubiquitin during the last step of the process (Budhidarmo et al., 2012). For this reason, we wanted to investigate the existence of physical interaction between the target substrate P-Rex1 and the Laforin-Malin complex. We performed this analysis by GFP-trap in HEK293 cells as indicated in Materials and Methods. In Figure 4A (lane 2), it can be observed that GFP-Malin was able to pulldown P-Rex1 and that this interaction was maintained in the presence of Flag-Laforin (lane 3). These findings suggest that P-Rex1 can interact with both Malin and Laforin. Similarly, in Figure 4B we can observe the physical interaction between Laforin and P-Rex1 (lane 2), that was maintained in the presence of Malin (lane 3) when the pulldown was performed using CFP-Laforin. These results confirmed that P-Rex1 can interact physically with Laforin and Malin both individually as well as when they are together in a complex.

Malin regulates P-Rex1 GEF activity on Rac1 GTPase

P-Rex1 belongs to the family of Rho guanine-nucleotide exchange factors (GEFs). They are structurally characterized by two types of catalytic domains (Dbl or DOCK) (Whitehead et al., 1997), (Machin et al., 2021), and are implicated in the activation of the components that belong to the Rac family of small GTPase proteins (Rac1, Rac2, Rac3, and RhoG), which can control several cellular responses (Wennerberg et al., 2005), (Hall, 1998). P-Rex1 carries the Dbl catalytic domain and, as a Rac-GEF, it favors the release of GDP from Rac that, in turn, will bind to free GTP and assume an active conformation. The active form of Rac, Rac-GTP, will promote its binding to downstream targets generating cellular responses (Cook et al., 2014), (Rossman et al., 2005). Previous studies reported that P-Rex1 can activate the different members of the Rac family of small GTPases both *in vitro* and *in vivo*, with the exception that, *in vivo*, the isoform of Rac that gets activated depends mostly on the cell type and the upstream signal that initiates the cascade of activation. Indeed, Rac-GEFs, like P-Rex1, have a very low basal activity and, to activate small GTPases like Rac, they need an upstream stimulus (Welch, 2015), (Welch et al., 2002).

Supported by these notions and by the work of other groups in demonstrating that P-Rex1 is an activator of Rac1 GTPase (Balamatsias et al., 2011), (Thamilselvan et al., 2020), one of our goals was to understand whether the ubiquitination of P-Rex1 by Malin could affect its activity as a Rac1-GEF. The first step was to confirm that P-Rex1 activates Rac1 GTPase in our cellular model. To measure Rac1 activation, a pulldown assay was performed, which involves the use of a GST fusion protein containing the Rac1 binding domain of PAK1 (GST-RBD-PAK1) known to interact with Rac1 only when the GTPase is in its active form (Arrizabalaga et al., 2012). To have a better readout for the activated forms of Rac1, we expressed exogenously an AU5-tagged Rac1 construct. In lane 3 of Fig. 5A, we can observe that the expression of P-Rex1 in HEK293 cells was necessary to produce activated forms of Rac1 GTPase, both endogenous and in the form of AU5-Rac1 (compare the intensity of the Rac1 bands in lane 3 with those present in the absence of P-Rex1; lanes 1 and 2) (see Fig. 5B for quantification). However, the expression of a functional Laforin-Malin complex produced a decrease in the amount of activated Rac1 GTPase forms (Fig. 5, lane 4; Fig. 5B). On the contrary, the expression of a non-functional Laforin-Malin complex, due to the presence of the Malin mutant form P69A, did not modify the level of activated forms of Rac1 present in lane 3 (Fig. 5, lane 5; Fig. 5B). Taken together, all these results lead us to hypothesize that the ubiquitination of P-Rex1 by Malin, through the introduction of polyubiquitin K63 chains, might result in a reduction in the activity of P-Rex1 as a Rac1-GEF. Next, we studied whether this effect could be due to an alteration in the stability of the protein due to its ubiquitination.

Malin-dependent ubiquitination of P-Rex1 reduces its protein stability

To establish whether the Malin-dependent ubiquitination of P-Rex1 could affect its protein stability we used primary astrocytes from the control and *Epm2b*−/− LD mouse model. Our group has already demonstrated that this LD mouse model recapitulates the hallmark of the disease (Rubio-Villena et al., 2018). We have used this model since P-Rex1 has been proven to be expressed at the level of the brain (Welch et al., 2002), (Yoshizawa et al., 2005), and primary astrocytes express enough levels of endogenous P-Rex1 to be detected by western blot using appropriate antibodies. So, we decided to measure its protein stability by subjecting primary astrocytes from control and *Epm2b*−/− mice to cycloheximide (CHX) treatment. The function of CHX is to block *de novo* protein synthesis and this allows us to evaluate the degradation rate of existing proteins following the initiation of the treatment. In this way, we can assess whether there is a difference in the degradation rate of the P-Rex1 substrate in control vs *Epm2b*−/− astrocytes. As we can see in Figure 6, in the control astrocytes we could appreciate the rate of degradation of the substrate starting from 12 hours of treatment with CHX. In comparison, at the same time point, in *Epm2b*−/− astrocytes the amount of P-Rex1 was higher, suggesting impairment in the rate of the degradation process due to the absence of Malin. After 24 h of CHX treatment, this difference in the degradation rate was still evident between control and *Epm2b*−/− samples. This result highlights the possibility that the Malin-dependent ubiquitination of endogenous P-Rex1 was responsible to direct P-Rex1 toward a degradative fate.

Increased glucose uptake in *Epm2b−/−* primary astrocytes

Then, we decided to focus on the physiological outcome of the longer half-life of P-Rex1 in *Epm2b−/−* astrocytes. In addition to the recognized role that P-Rex1 has in cancer (Srijakotre et al., 2020), (Qiu et al., 2020), (Beltran-Navarro et al., 2022), it also plays a role in glucose homeostasis (Moller et al., 2019), (Machin et al., 2021). In this sense, it has been demonstrated that P-Rex1 promotes the translocation of the glucose transporter GLUT4 to the plasma membrane on 3T3-L1 adipocytes cells (Balamatsias et al., 2011). Supported by these data, we compared the rate of glucose uptake in primary astrocytes from control and *Epm2b−/−* mice, as described in Materials and Methods. As a control, we treated astrocytes with metformin, a compound known to increase glucose uptake (Polianskyte-Prause et al., 2019). As can be observed in Fig. 7A, we found higher glucose uptake in astrocytes from *Epm2b−/−* than in controls. Treatment with metformin increased glucose uptake in control, and *Epm2b−/−* astrocytes.

In order to assess for the possible connection between P-Rex1 and glucose uptake in *Epm2b−/−* astrocytes we decided to silence the expression of P-Rex1 in these cells. As it is indicated in Fig. 7B, the silencing of P-Rex1 in *Epm2b−/−* astrocytes resulted in a statistically significant decrease in glucose uptake. Silencing of control astrocytes also showed a tendency to decrease glucose uptake (Fig. 7C confirms the reduction in P-Rex1 expression upon silencing). These results suggest a close relationship between the levels of P-Rex1 and the capacity to uptake glucose.

Next, we wanted to check if the increase in glucose uptake in *Epm2b−/−* astrocytes was due to higher levels of glucose transporters at the plasma membrane. With this aim, we used the Pierce Cell Surface Protein Isolation Kit, which consists in treating the cells with EZ-LINK Sulfo-NHS-SS-biotin that will bind to the proteins of the plasma membrane. The biotinylated protein fraction, corresponding only to plasma membrane proteins, is then isolated with NeutrAvidin beads. We analyzed the presence of GLUT1, the main glucose transporter present in astrocytes, in the purified fraction by using GLUT1-specific antibodies. As shown in Fig. 7D, the purified biotinylated fraction of plasma membrane proteins was enriched in the Na+/K+-ATPase (lower panel), a regular plasma membrane protein, and decreased in the levels of actin, a cytosolic marker (middle panel). However, we did not observe any difference in the levels of the glycosylated (55 kDa) or the non-glycosylated (45 kDa) forms of GLUT1 between control and *Epm2b−/−* astrocytes (Fig. 7D upper panel, and 7E). Taken together, these results indicate that the differences in glucose uptake that we observed in *Epm2b−/−* compared to control must depend probably on the increased activity of the glucose transporter rather than on changes in its protein levels at the cell surface.

DISCUSSION

Several groups, including ours, have widely described how Lafora disease occurs due to the alteration of the functionality of the Laforin-Malin complex. However, more studies are needed to deeply understand Lafora disease pathophysiology. One strategy to pursue this objective lies in seeking factors that are altered at the molecular level. As a result of the role of Malin in LD, it is well-establish that the disease presents a compromised

ubiquitination process, and this contributes to the onset of many dysfunctions. The discovery of substrates that fail to be ubiquitinated by Malin in LD sets an attempt in trying to explain the occurrence of some alterations distinctive to the disease. For this reason, the first step of this work was to identify new candidate substrates of Malin through an unbiased approach based on the activity of Malin as an E3-ubiquitin ligase by using the ^{bio}Ub strategy (Martinez et al., 2017), (Ramirez et al., 2018). This procedure allowed the enrichment and isolation of ubiquitin conjugates present in cells expressing Malin-WT or an inactive form of Malin (P69A). Subsequently, by proteomic analysis, we were able to discover a series of candidates that were differentially ubiquitinated. An informatics analysis of these proteins indicated that the biological processes in which they were involved were mostly protein folding, response to heat shock, and regulation of mitochondrial function (Fig. 2B, top panel) and their molecular functions were heat shock proteins and ubiquitin ligases (Fig. 2B, bottom panel). These analyses also indicated that most of them clustered in two groups, the heat shock protein (HSPs) group and the OXPHOS group (Fig. 2C) (Table 1). We were expecting to see at least some of the proteins involved in glycogen biosynthesis/regulation, but none of them passed the stringent filters we established for our bioUb strategy to identify ubiquitination candidates. We can only speculate by saying that perhaps the glycogen-related proteins had lower rates of ubiquitination in comparison to the rest of the identified proteins, and/or that the levels of these proteins were lower in comparison to the more abundant modified proteins present in the cells. In any case, our results are in agreement with reports in the literature that indicates that Malin interacts with different heat shock proteins by yeast two-hybrid or co-immunoprecipitation (Garyali et al., 2009), (Rao et al., 2010a), (Rao et al., 2010b), (Sun et al., 2019).

Among these candidates, P-Rex1 prevailed in terms of ubiquitination rate (more than 18-fold) (Table 1). Next, we progressed in the validation of the substrate: the ubiquitination assay shows clear ubiquitination of P-Rex1 by the regular Laforin-Malin complex while, in the presence of the inactive form of Malin, the post-translational modification on the substrate was decreased. In addition, we also addressed the inclination of Malin in introducing K63-type polyubiquitin chains, as in the case of other substrates described in previous reports by us and other groups [see (Garcia-Gimeno et al., 2018) for review]. This Malin-dependent ubiquitination of P-Rex1 was favored by a physical protein-protein interaction between the Laforin/Malin complex and P-Rex1.

In terms of function, P-Rex1 is a Rac-GEF that activates GTPases that are in their inactive state. One of the well-known GTPases that have been described to be activated by P-Rex1 is Rac1 (Balamatsias et al., 2011), (Thamilselvan et al., 2020). In this regard, we aimed to understand whether the Laforin-Malin complex could modulate the activity of P-Rex1 on Rac1. By measuring the activation of Rac1 in HEK293 cells we confirmed that P-Rex1 was capable of activating Rac1, and more importantly, we showed that the Laforin/Malin complex prevented the activation of Rac1 in these cells. On the contrary, the expression of an inactive Laforin/Malin complex (containing the Malin P69A form) did not affect the levels of activated forms of Rac1. Of note, we would like to point out that it is the first time that the activity of a GEF of Rac1 could be modulated by ubiquitination, in contrast to the most known modulation of GEF activity by phosphorylation (Crespo et al., 1997), (Llavero et al., 2015).

These results led us to consider that the ubiquitination of P-Rex1 by Malin affected the stability of the protein and perhaps targeted the substrate toward degradation. To sustain this concept, we had to move our experimental approach to a cellular system where the levels of endogenous P-Rex1 were measurable since HEK293 cells express very low levels of this protein. For this reason, we used primary cultures of astrocytes from control and *Epm2b*−/− mice. By treating these cells with cycloheximide (an inhibitor of *de novo* protein synthesis) we concluded that the degradation rate of the substrate in *Epm2b*−/− primary astrocytes was lower compared to control astrocytes. This allowed us to suggest that in the absence of Malin, the degradation rate of P-Rex1 decreases, probably because of defective ubiquitination of the substrate.

Since it has been demonstrated that P-Rex1 has a role in glucose homeostasis (Moller et al., 2019), (Machin et al., 2021), as it promotes the translocation of the glucose transporter GLUT4 to the plasma membrane on 3T3-L1 adipocytes cells (Balamatsias et al., 2011), we analyzed glucose uptake in astrocytes from control and *Epm2b*−/− mice. We observed higher uptake of glucose in *Epm2b*−/− astrocytes, suggesting that the absence of Malin enhances the transport of glucose inside the cell. This increase could be partially due to the action of P-Rex1 in these cells since when we decreased its expression by siRNA, we observed a decrease in glucose uptake.

As GLUT1 is the main glucose transporter present in astrocytes (Koepsell, 2020), and there are recent reports that indicate that GLUT1, in addition to being located at the plasma membrane, is also present in intracellular deposits that serve as reservoirs of GLUT1, to be translocated to the plasma membrane under stress conditions (Wu et al., 2013), (Muraleedharan et al., 2020), we decided to check whether P-Rex1 could regulate GLUT1 translocation as it does for GLUT4 in adipocytes. However, in our cellular system (astrocytes) we were not able to detect changes in the levels of the glucose transporter GLUT1 at the level of the plasma membrane. We also checked for the presence of GLUT3 and GLUT4 in the purified plasma membrane fraction but, since the expression of these isoforms is very low in astrocytes (Koepsell, 2020), we were not able to detect any signal (data not shown). So, we concluded that the absence of Malin in astrocytes could affect the activity of the glucose transporters and not their levels at the plasma membrane. It is worth pointing out that the activity of GLUT1 changes depending on its location in specific areas of the plasma membrane (lipid rafts) (Koepsell, 2020). So we can speculate that the increase in glucose uptake observed in the absence of Malin could be partially due to the action of P-Rex1 at the plasma membrane.

In any case, our results indicate that glucose uptake is increased in *Epm2b*−/− astrocytes, and this could be one of the reasons for the characteristic accumulation of glycogen in LD. Therefore, any strategy aimed to decrease glucose uptake will be beneficial since it will decrease glycogen production. This therapeutic strategy has been already proved with the use of trehalose, a disaccharide that blocks glucose transport (Mardones et al., 2016), as it has been reported that the administration of trehalose to LD mouse models ameliorates seizure susceptibility (Sinha et al., 2021).

ACKNOWLEDGMENTS

We want to thank Dr. Atanasio Pandiella (CIC-Salamanca), Dr. Manuel Rodríguez (Proteomics Unit. CIC-bioGUNE. Bizkaia. Spain), and Dr. Ch. Blattner (Institute of Toxicology and Genetics. Karlsruhe Institute of Technology. Karlsruhe. Germany) for plasmids. We also thank the support provided by SGIker Proteomics service (UPV/EHU - ERDF. EU). This work has received funding from the European Union's Horizon 2020 research and innovation program under the Marie Sklodowska-Curie grant agreement 813599 (TRIM-NET). We also want to acknowledge the support of the grant from the National Institutes of Health P01 NS097197, which established the Lafora Epilepsy Cure Initiative (LECI), and a grant from la Fundació La Marató TV3 (202032), to PS; and a grant from the Spanish Ministry of Science and Innovation PID2020–112972RB-I00 to PS and MGG.

REFERENCES

Aguado C, et al. , 2010. Laforin, the most common protein mutated in Lafora disease, regulates autophagy. Hum Mol Genet. 19, 2867–76. [PubMed: 20453062]

Ahonen S, et al. , 2021. Gys1 antisense therapy rescues neuropathological bases of murine Lafora disease. Brain. 144, 2985–2993. [PubMed: 33993268]

Arrizabalaga O, et al. , 2012. Rac1 protein regulates glycogen phosphorylase activation and controls interleukin (IL)-2-dependent T cell proliferation. J Biol Chem. 287, 11878–90. [PubMed: 22337875]

Balamatsias D, et al. , 2011. Identification of P-Rex1 as a novel Rac1-guanine nucleotide exchange factor (GEF) that promotes actin remodeling and GLUT4 protein trafficking in adipocytes. J Biol Chem. 286, 43229–40. [PubMed: 22002247]

Beltran-Navarro YM, et al. , 2022. P-Rex1 Signaling Hub in Lower Grade Glioma Patients, Found by In Silico Data Mining, Correlates With Reduced Survival and Augmented Immune Tumor Microenvironment. Front Oncol. 12, 922025. [PubMed: 35875157]

Brewer MK, Gentry MS, 2019. Brain Glycogen Structure and Its Associated Proteins: Past, Present and Future. Adv Neurobiol. 23, 17–81. [PubMed: 31667805]

Budhidarmo R, et al. , 2012. RINGs hold the key to ubiquitin transfer. Trends Biochem Sci. 37, 58–65. [PubMed: 22154517]

Cook DR, et al. , 2014. Rho guanine nucleotide exchange factors: regulators of Rho GTPase activity in development and disease. Oncogene. 33, 4021–35. [PubMed: 24037532]

Couarch P, et al. , 2011. Lafora progressive myoclonus epilepsy: NHLRC1 mutations affect glycogen metabolism. J Mol Med (Berl). 89, 915–25. [PubMed: 21505799]

Cox J, Mann M, 2008. MaxQuant enables high peptide identification rates, individualized p.p.b.-range mass accuracies and proteome-wide protein quantification. Nat Biotechnol. 26, 1367–72. [PubMed: 19029910]

Crespo P, et al. , 1997. Phosphotyrosine-dependent activation of Rac-1 GDP/GTP exchange by the vav proto-oncogene product. Nature. 385, 169–72. [PubMed: 8990121]

Chan EM, et al. , 2003. Mutations in NHLRC1 cause progressive myoclonus epilepsy. Nat Genet. 35, 125–7. [PubMed: 12958597]

Cheng A, et al. , 2007. A role for AGL ubiquitination in the glycogen storage disorders of Lafora and Cori's disease. Genes Dev. 21, 2399–409. [PubMed: 17908927]

Elu N, et al. , 2020. Mass Spectrometry-Based Characterization of Ub- and UbL-Modified Proteins. Methods Mol Biol. 2051, 265–276. [PubMed: 31552633]

Elu N, et al. , 2019. Detailed Dissection of UBE3A-Mediated DDI1 Ubiquitination. Front Physiol. 10, 534. [PubMed: 31130875]

Franco M, et al. , 2011. A novel strategy to isolate ubiquitin conjugates reveals wide role for ubiquitination during neural development. Mol Cell Proteomics. 10, M110 002188.

Garcia-Gimeno MA, et al. , 2018. Lafora Disease: A Ubiquitination-Related Pathology. Cells. 7, 87. [PubMed: 30050012]

Garyali P, et al. , 2009. The malin-laforin complex suppresses the cellular toxicity of misfolded proteins by promoting their degradation through the ubiquitin-proteasome system. Hum Mol Genet. 18, 688–700. [PubMed: 19036738]

Gentry MS, et al. , 2005. Insights into Lafora disease: malin is an E3 ubiquitin ligase that ubiquitinates and promotes the degradation of laforin. Proc Natl Acad Sci U S A. 102, 8501–6. [PubMed: 15930137]

Hall A, 1998. Rho GTPases and the actin cytoskeleton. Science. 279, 509–14. [PubMed: 9438836]

Hatakeyama S, 2017. TRIM Family Proteins: Roles in Autophagy, Immunity, and Carcinogenesis. Trends Biochem Sci. 42, 297–311. [PubMed: 28118948]

Hertz L, et al. , 1998. Functional studies in cultured astrocytes. Methods. 16, 293–310. [PubMed: 10071068]

Kaiser P, Tagwerker C, Is This Protein Ubiquitinated? Elsevier, 2005, pp. 243–248.

Kalviainen R, 2015. Progressive Myoclonus Epilepsies. Semin Neurol. 35, 293–9. [PubMed: 26060909]

Koepsell H, 2020. Glucose transporters in brain in health and disease. Pflugers Arch. 472, 1299–1343. [PubMed: 32789766]

Komander D, Rape M, 2012. The ubiquitin code. Annu Rev Biochem. 81, 203–29. [PubMed: 22524316]

Kumarasinghe L, et al. , 2021. TRIM32 and Malin in Neurological and Neuromuscular Rare Diseases. Cells. 10, 820. [PubMed: 33917450]

Lafora GR, Glueck B, 1911. Beitrag zur Histopathologie der myoklonischen Epilepsie. Zeitschrift für die gesamte Neurologie und Psychiatrie. 6, 1–14.

Lahuerta M, et al. , 2018. Degradation of altered mitochondria by autophagy is impaired in Lafora disease. FEBS J. 285, 2071–2090. [PubMed: 29645350]

Lahuerta M, et al. , 2020. Reactive Glia-Derived Neuroinflammation: a Novel Hallmark in Lafora Progressive Myoclonus Epilepsy That Progresses with Age. Mol Neurobiol. 57, 1607–1621. [PubMed: 31808062]

Lectez B, et al. , 2014. Ubiquitin profiling in liver using a transgenic mouse with biotinylated ubiquitin. J Proteome Res. 13, 3016–26. [PubMed: 24730562]

Lopez-Gonzalez I, et al. , 2017. Inflammation in Lafora Disease: Evolution with Disease Progression in Laforin and Malin Knock-out Mouse Models. Mol Neurobiol. 54, 3119–3130. [PubMed: 27041370]

Llavero F, et al. , 2015. Guanine nucleotide exchange factor alphaPIX leads to activation of the Rac 1 GTPase/glycogen phosphorylase pathway in interleukin (IL)-2-stimulated T cells. J Biol Chem. 290, 9171–82. [PubMed: 25694429]

Machin PA, et al. , 2021. Rho Family GTPases and Rho GEFs in Glucose Homeostasis. Cells. 10, 915. [PubMed: 33923452]

Magistretti PJ, et al. , 1983. Functional receptors for vasoactive intestinal polypeptide in cultured astroglia from neonatal rat brain. Regul Pept. 6, 71–80. [PubMed: 6306734]

Mallette FA, Richard S, 2012. K48-linked ubiquitination and protein degradation regulate 53BP1 recruitment at DNA damage sites. Cell Res. 22, 1221–3. [PubMed: 22491476]

Mardones P, et al. , 2016. Mystery solved: Trehalose kickstarts autophagy by blocking glucose transport. Sci Signal. 9, 416.

Martinez A, et al. , 2017. Quantitative proteomic analysis of Parkin substrates in Drosophila neurons. Mol Neurodegener. 12, 29. [PubMed: 28399880]

Meroni G, 2020. TRIM E3 Ubiquitin Ligases in Rare Genetic Disorders. Adv Exp Med Biol. 1233, 311–325. [PubMed: 32274764]

Meroni G, Desagher S, 2022. Cellular Function of TRIM E3 Ubiquitin Ligases in Health and Disease. Cells. 11, 250. [PubMed: 35053366]

Minassian BA, et al. , 1998. Mutations in a gene encoding a novel protein tyrosine phosphatase cause progressive myoclonus epilepsy. Nat Genet. 20, 171–4. [PubMed: 9771710]

Moller LLV, et al. , 2019. Rho GTPases-Emerging Regulators of Glucose Homeostasis and Metabolic Health. Cells. 8, 434. [PubMed: 31075957]

Moreno D, et al. , 2010. The laforin-malin complex, involved in Lafora disease, promotes the incorporation of K63-linked ubiquitin chains into AMP-activated protein kinase beta subunits. Mol Biol Cell. 21, 2578–88. [PubMed: 20534808]

Muller MS, et al. , 2014. Astrocyte glycogenolysis is triggered by store-operated calcium entry and provides metabolic energy for cellular calcium homeostasis. Glia. 62, 526–34. [PubMed: 24464850]

Munoz-Ballester C, et al. , 2016. Homeostasis of the astrocytic glutamate transporter GLT-1 is altered in mouse models of Lafora disease. Biochim Biophys Acta. 1862, 1074–1083. [PubMed: 26976331]

Muraleedharan R, et al. , 2020. AMPK-Regulated Astrocytic Lactate Shuttle Plays a Non-Cell-Autonomous Role in Neuronal Survival. Cell Rep. 32, 108092. [PubMed: 32877674]

Osinalde N, et al. , 2015. SILAC-based quantification of changes in protein tyrosine phosphorylation induced by Interleukin-2 (IL-2) and IL-15 in T-lymphocytes. Data Brief. 5, 53–8. [PubMed: 26425665]

Pederson BA, et al. , 2013. Inhibiting glycogen synthesis prevents Lafora disease in a mouse model. Ann Neurol. 74, 297–300. [PubMed: 23913475]

Perez-Jimenez E, et al. , 2021. Endocytosis of the glutamate transporter 1 is regulated by laforin and malin: Implications in Lafora disease. Glia. 69, 1170–1183. [PubMed: 33368637]

Pirone L, et al. , 2017. A comprehensive platform for the analysis of ubiquitin-like protein modifications using in vivo biotinylation. Sci Rep. 7, 40756. [PubMed: 28098257]

Polianskyte-Prause Z, et al. , 2019. Metformin increases glucose uptake and acts renoprotectively by reducing SHIP2 activity. FASEB J. 33, 2858–2869. [PubMed: 30321069]

Pondrelli F, et al. , 2021. Natural history of Lafora disease: a prognostic systematic review and individual participant data meta-analysis. Orphanet J Rare Dis. 16, 362. [PubMed: 34399803]

Puri R, Ganesh S, 2012. Autophagy defects in Lafora disease: cause or consequence? Autophagy. 8, 289–90. [PubMed: 22301990]

Qiu W, et al. , 2020. Identification of P-Rex1 in the Regulation of Liver Cancer Cell Proliferation and Migration via HGF/c-Met/Akt Pathway. Onco Targets Ther. 13, 9481–9495. [PubMed: 33061433]

Ramirez J, et al. , 2018. Quantitative proteomics reveals neuronal ubiquitination of Rngo/Ddi1 and several proteasomal subunits by Ube3a, accounting for the complexity of Angelman syndrome. Hum Mol Genet. 27, 1955–1971. [PubMed: 29788202]

Ramirez J, et al. , 2015. Proteomic Analysis of the Ubiquitin Landscape in the Drosophila Embryonic Nervous System and the Adult Photoreceptor Cells. PLoS One. 10, e0139083. [PubMed: 26460970]

Ramirez J, et al. , 2021a. The ubiquitin ligase Ariadne-1 regulates neurotransmitter release via ubiquitination of NSF. J Biol Chem. 296, 100408. [PubMed: 33581113]

Ramirez J, et al. , 2021b. A Proteomic Approach for Systematic Mapping of Substrates of Human Deubiquitinating Enzymes. Int J Mol Sci. 22, 4851. [PubMed: 34063716]

Rao SN, et al. , 2010a. Sequestration of chaperones and proteasome into Lafora bodies and proteasomal dysfunction induced by Lafora disease-associated mutations of malin. Hum Mol Genet. 19, 4726–34. [PubMed: 20858601]

Rao SN, et al. , 2010b. Co-chaperone CHIP stabilizes aggregate-prone malin, a ubiquitin ligase mutated in Lafora disease. J Biol Chem. 285, 1404–13. [PubMed: 19892702]

Reymond A, et al. , 2001. The tripartite motif family identifies cell compartments. EMBO J. 20, 2140–51. [PubMed: 11331580]

Riva A, et al. , 2021. Italian cohort of Lafora disease: Clinical features, disease evolution, and genotype-phenotype correlations. J Neurol Sci. 424, 117409. [PubMed: 33773408]

Roma-Mateo C, et al. , 2015a. Increased oxidative stress and impaired antioxidant response in lafora disease. Mol Neurobiol. 51, 932–46. [PubMed: 24838580]

Roma-Mateo C, et al. , 2015b. Oxidative stress, a new hallmark in the pathophysiology of Lafora progressive myoclonus epilepsy. Free Radic Biol Med. 88, 30–41. [PubMed: 25680286]

Roma-Mateo C, et al. , 2011. Laforin, a dual-specificity phosphatase involved in Lafora disease, is phosphorylated at Ser25 by AMP-activated protein kinase. Biochem J. 439, 265–75. [PubMed: 21728993]

Rossman KL, et al. , 2005. GEF means go: turning on RHO GTPases with guanine nucleotide-exchange factors. Nat Rev Mol Cell Biol. 6, 167–80. [PubMed: 15688002]

Rubio-Villena C, et al. , 2013. Glycogenic activity of R6, a protein phosphatase 1 regulatory subunit, is modulated by the laforin-malin complex. Int J Biochem Cell Biol. 45, 1479–88. [PubMed: 23624058]

Rubio-Villena C, et al. , 2018. Astrocytes: new players in progressive myoclonus epilepsy of Lafora type. Hum Mol Genet. 27, 1290–1300. [PubMed: 29408991]

Sakai M, et al. , 1970. Studies in myoclonus epilepsy (Lafora body form). II. Polyglucosans in the systemic deposits of myoclonus epilepsy and in corpora amylacea. Neurology. 20, 160–76. [PubMed: 4188951]

Sanchez-Martin P, et al. , 2020. Regulation of the autophagic PI3KC3 complex by laforin/malin E3-ubiquitin ligase, two proteins involved in Lafora disease. Biochim Biophys Acta Mol Cell Res. 1867, 118613. [PubMed: 31758957]

Sanchez-Martin P, et al. , 2015. Ubiquitin conjugating enzyme E2-N and sequestosome-1 (p62) are components of the ubiquitination process mediated by the malin-laforin E3-ubiquitin ligase complex. Int J Biochem Cell Biol. 69, 204–14. [PubMed: 26546463]

Serratosa JM, et al. , 1999. A novel protein tyrosine phosphatase gene is mutated in progressive myoclonus epilepsy of the Lafora type (EPM2). Hum Mol Genet. 8, 345–52. [PubMed: 9931343]

Sharma J, et al. , 2012. Malin Regulates Wnt Signaling Pathway through Degradation of Dishevelled2. J Biol Chem. 287, 6830–9. [PubMed: 22223637]

Singh PK, et al. , 2012. The Laforin-Malin Complex Negatively Regulates Glycogen Synthesis by Modulating Cellular Glucose Uptake via Glucose Transporters. Mol Cell Biol. 32, 652–63. [PubMed: 22124153]

Sinha P, et al. , 2021. Trehalose Ameliorates Seizure Susceptibility in Lafora Disease Mouse Models by Suppressing Neuroinflammation and Endoplasmic Reticulum Stress. Mol Neurobiol. 58, 1088–1101. [PubMed: 33094475]

Solaz-Fuster MC, et al. , 2008. Regulation of glycogen synthesis by the laforin–malin complex is modulated by the AMP-activated protein kinase pathway. Human Molecular Genetics. 17, 667–678. [PubMed: 18029386]

Srijakotre N, et al. , 2020. PtdIns(3,4,5)P3-dependent Rac exchanger 1 (P-Rex1) promotes mammary tumor initiation and metastasis. Proc Natl Acad Sci U S A. 117, 28056–28067. [PubMed: 33097662]

Sun RC, et al. , 2019. Nuclear Glycogenolysis Modulates Histone Acetylation in Human Non-Small Cell Lung Cancers. Cell Metab. 30, 903–916 e7. [PubMed: 31523006]

Swatek KN, Komander D, 2016. Ubiquitin modifications. Cell Res. 26, 399–422. [PubMed: 27012465]

Thamilselvan V, et al. , 2020. P-Rex1 Mediates Glucose-Stimulated Rac1 Activation and Insulin Secretion in Pancreatic beta-Cells. Cell Physiol Biochem. 54, 1218–1230. [PubMed: 33347743]

Turnbull J, et al. , 2011. PTG depletion removes Lafora bodies and rescues the fatal epilepsy of Lafora disease. PLoS Genet. 7, e1002037. [PubMed: 21552327]

Turnbull J, et al. , 2014. PTG protein depletion rescues malin-deficient Lafora disease in mouse. Ann Neurol. 75, 442–6. [PubMed: 24419970]

Turnbull J, et al. , 2012. Early-onset Lafora body disease. Brain. 135, 2684–2698. [PubMed: 22961547]

Turnbull J, et al. , 2016. Lafora disease. Epileptic Disorders. 18, 38–62. [PubMed: 27702709]

Tyanova S, et al. , 2016. The Perseus computational platform for comprehensive analysis of (prote)omics data. Nat Methods. 13, 731–40. [PubMed: 27348712]

Viana R, et al. , 2015. The laforin/malin E3-ubiquitin ligase complex ubiquitinates pyruvate kinase M1/M2. BMC Biochem. 16, 24. [PubMed: 26493215]

Welch HC, 2015. Regulation and function of P-Rex family Rac-GEFs. Small GTPases. 6, 49–70. [PubMed: 25961466]

Welch HC, et al. , 2002. P-Rex1, a PtdIns(3,4,5)P3- and Gbetagamma-regulated guanine-nucleotide exchange factor for Rac. Cell. 108, 809–21. [PubMed: 11955434]

Wennerberg K, et al. , 2005. The Ras superfamily at a glance. J Cell Sci. 118, 843–6. [PubMed: 15731001]

Whitehead IP, et al. , 1997. Dbl family proteins. Biochim Biophys Acta. 1332, F1–23. [PubMed: 9061011]

Wu N, et al. , 2013. AMPK-dependent degradation of TXNIP upon energy stress leads to enhanced glucose uptake via GLUT1. Mol Cell. 49, 1167–75. [PubMed: 23453806]

Yoshizawa M, et al. , 2005. Involvement of a Rac activator,P-Rex1, in neurotrophin-derived signaling and neuronal migration. J Neurosci. 25, 4406–19. [PubMed: 15858067]

Highlights:

- Comparative proteomics of ubiquitinated proteins defines novel Malin substrates.
- The Laforin/Malin complex binds and ubiquitinates P-Rex1, a GEF of the Rac1 family.
- Ubiquitination of P-Rex1 affects its activity as a Rac1-GEF.
- In the absence of Malin, P-Rex1 has a longer half-life, improving glucose uptake.

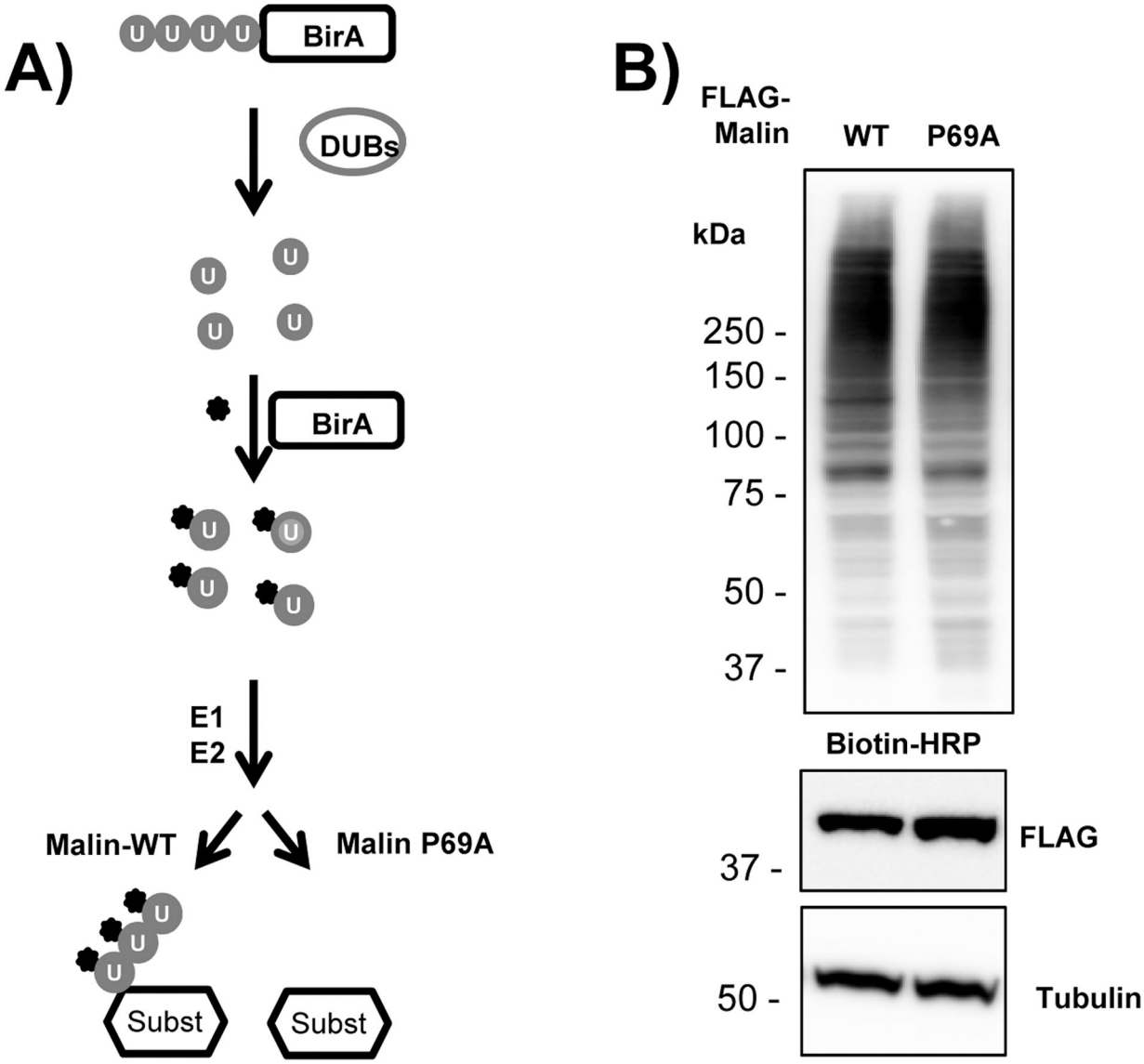

Fig. 1: Strategy for the analysis of Malin-dependent differentially ubiquitinated substrates.

A) Diagram of the experimental reaction. See text for details. DUBs: endogenous deubiquitinating enzymes; U: ubiquitin; BirA: *E.coli* biotin ligase; biotin is depicted in black. B) Ubiquitinated status of cell extracts. HEK293 cells were transfected with plasmids expressing bioUb-BirA and FLAG-Malin WT or the inactive form FLAG-Malin P69A. 30 μg of cell extracts were analyzed by western blot using anti-biotin-HRP-conjugated, anti-FLAG, and anti-tubulin antibodies. Molecular weight markers are indicated on the left.

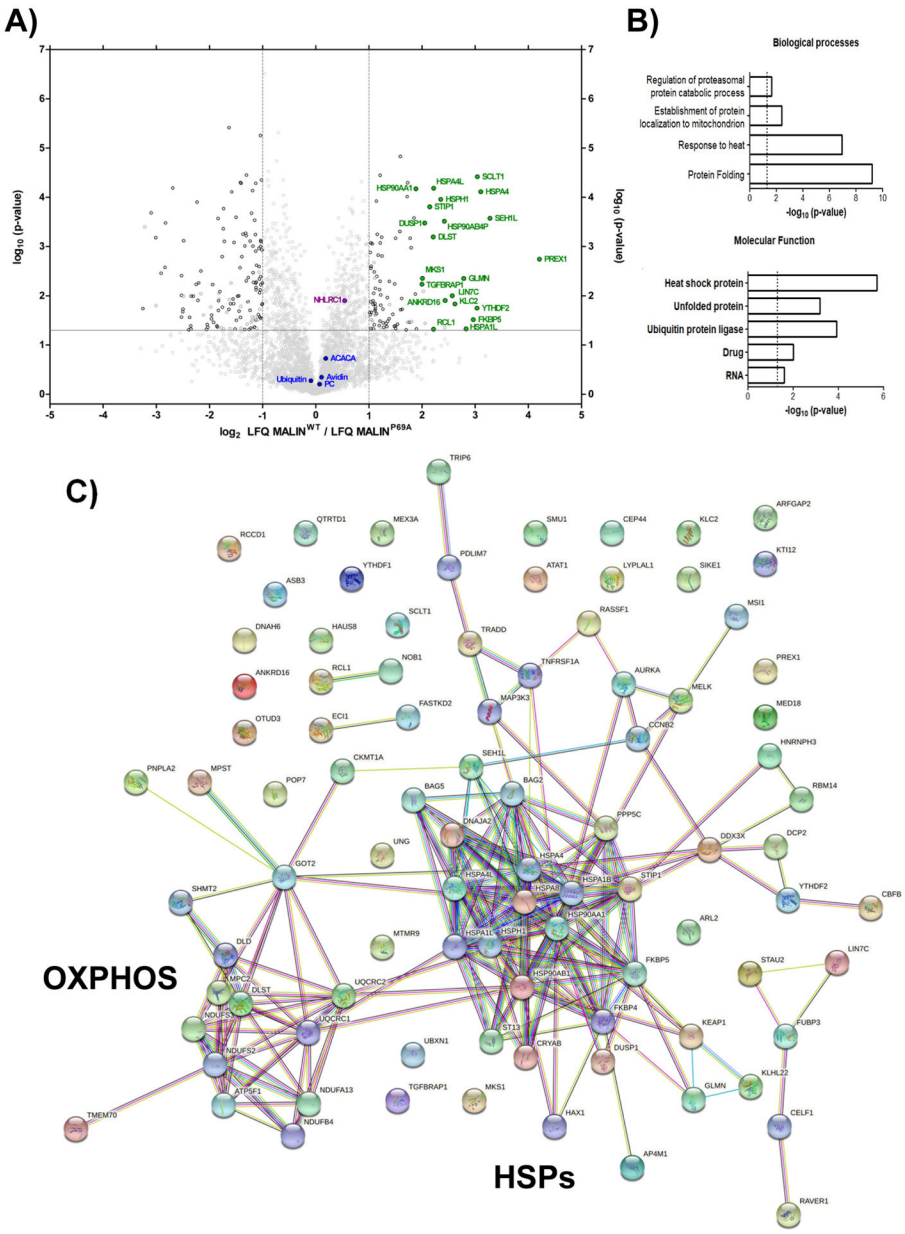

Fig. 2: *In silico* analysis of the Malin-dependent ubiquitinated proteins.

A) Identification of candidate Malin substrates. Comparison of the abundance of the ubiquitinated proteins identified by MS upon Malin WT overexpression relative to cells overexpressing the Malin P69A mutant. Three independent samples from each case were analyzed. The volcano plot displays the LFQ Malin-WT/Malin-P69A ratios on $\log_2$ scale (*X*-axis) and the t-test P-values on $-\log_{10}$ scale (*Y*-axis). Malin candidate substrates with a significant (P-value < 0.05) LFQ Malin-WT/Malin-P69A ratio higher than 4 are labelled in green. The ACACA and PC carboxylases, which use biotin as a cofactor, Ubiquitin, and the Avidin used for the pulldowns are labelled in blue. The Malin protein (NHLRC1) is labelled in magenta. A horizontal grey lane determines the statistical significance, while the vertical dashed lines determine a two-fold enrichment. B) DAVID analysis of the identified proteins.

The grouped biological processes and molecular functions of the proteins are indicated. C) STRING analysis of the same set of proteins. Two major groups were identified, the heat shock protein (HSPs) group and the mitochondrial oxidative phosphorylation (OXPHOS) group.

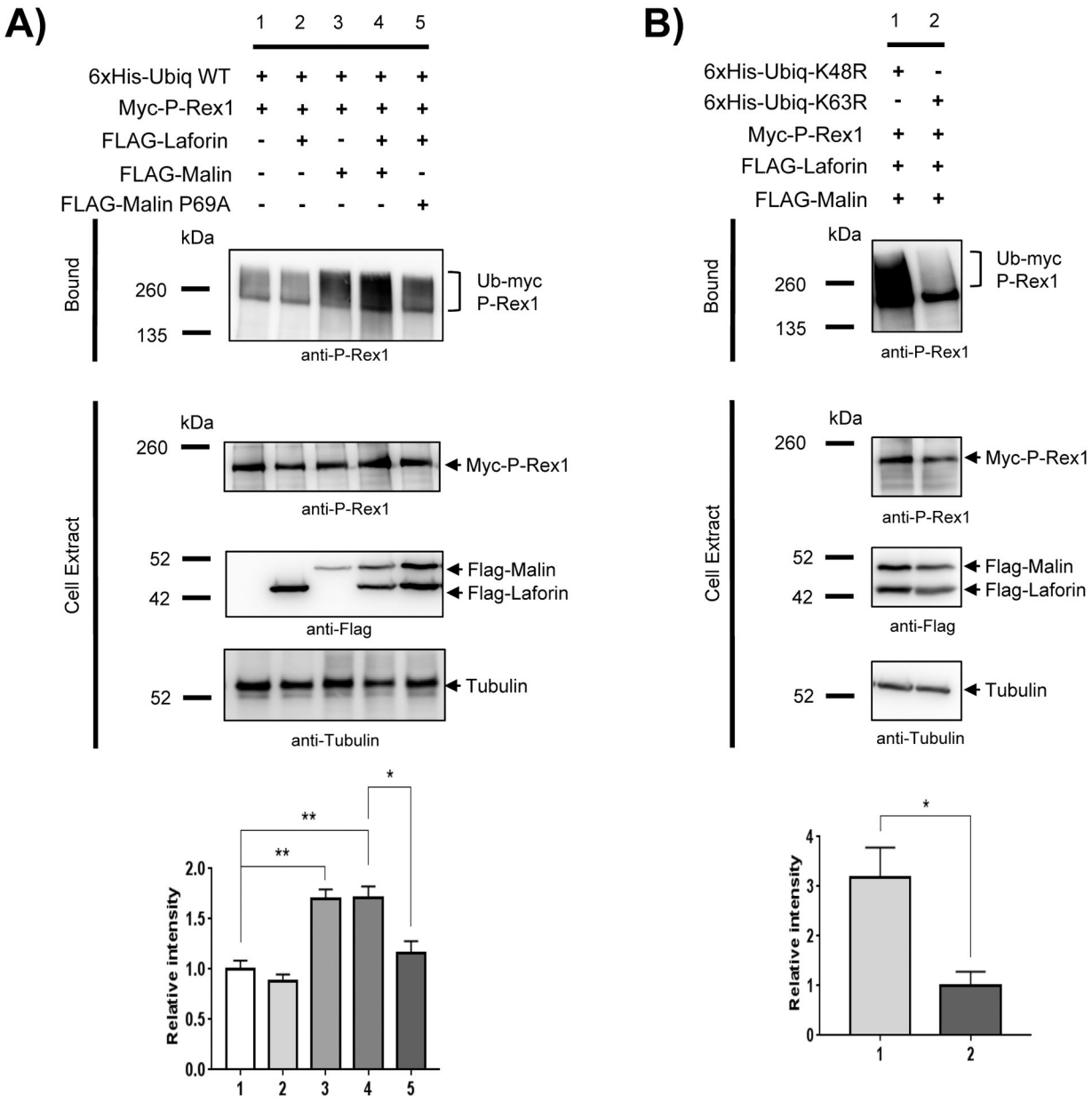

Fig. 3: Validation of P-Rex1 as a substrate of Malin.

A) A functional Laforin/Malin complex ubiquitinates P-Rex1. HEK293 cells were transfected with the indicated plasmids and the ubiquitination analysis of P-Rex1 was performed as described in Materials and Methods. The analyses were carried out with wild type and inactive (P69A) forms of Malin. Proteins present in the bound fraction (Bound: proteins retained in the metal affinity resin) or in the crude cell extract (50 μg) were analyzed by Western blotting using the indicated antibodies. The lower panel shows the quantification of the ubiquitination signal referred to the signal observed in cells expressing only myc-P-Rex1 (lane 1), which was adjusted to 1. B) Topology of the ubiquitination reaction. Ubiquitination reactions were performed as in A) using modified forms of ubiquitin that carried K48R or K63R mutations, which prevent the formation of

K48- or K63-linked chains, respectively. The lower panel shows the quantification of the ubiquitination signal referred to the signal observed in cells expressing K63R-ubiquitin (lane 2), which was adjusted to 1. Values are the mean +/− SEM of three independent experiments (*p<0.05; **p<0.01).

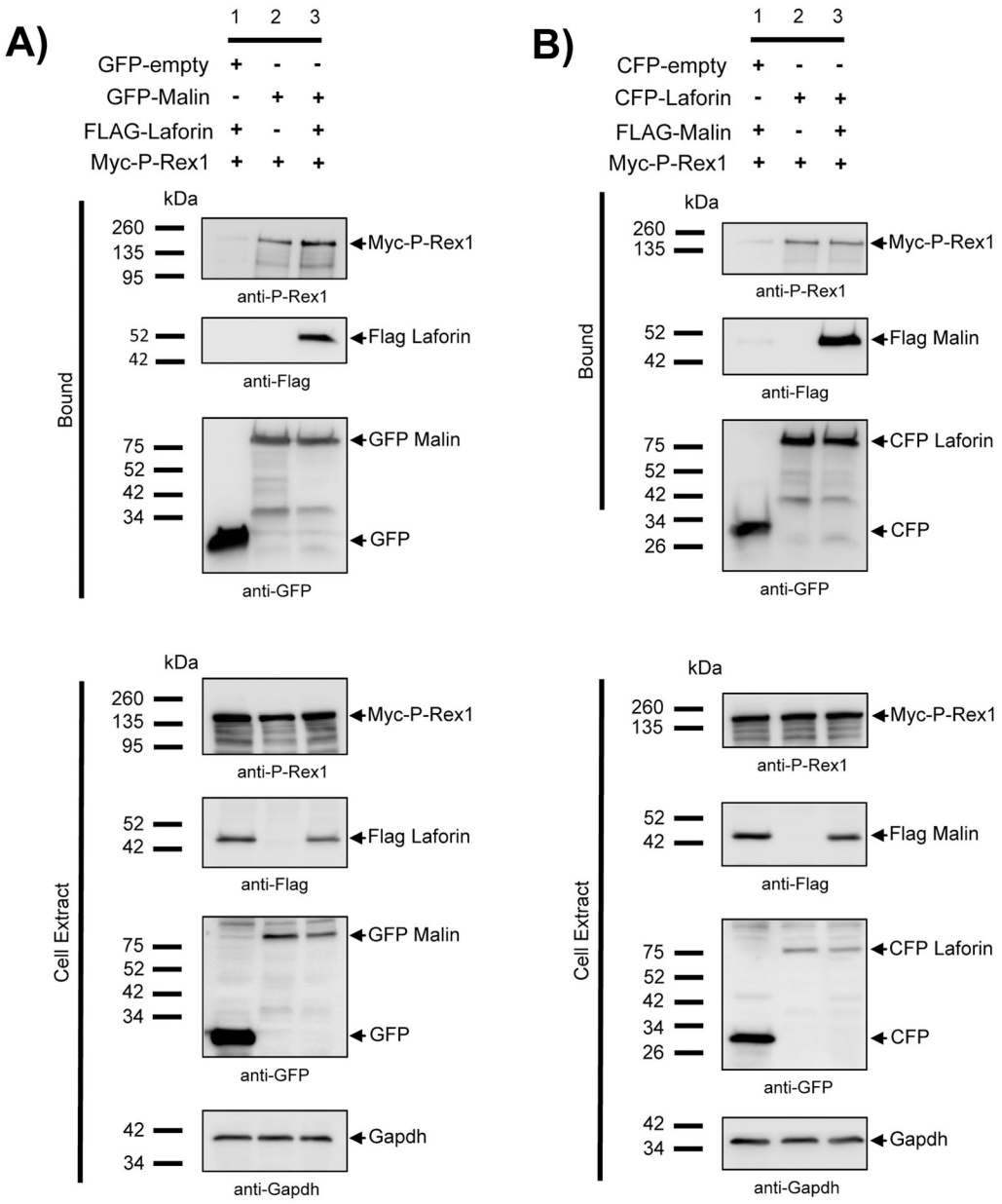

Fig. 4: The Laforin-Malin complex interacts physically with P-Rex1.

A) GFP-Malin pull-downs P-Rex1. HEK293 cells were co-transfected with the indicated combination of plasmids expressing Myc-P-Rex1, FLAG-Laforin, GFP (empty), and GFP-Malin. Cells were lysed and 1.5 mg of proteins were incubated with GFP-trap beads. which bind the various GFP forms with high affinity. After washing, beads were boiled in loading buffer and the purified proteins were analyzed by SDS-PAGE and Western blot using anti-GFP. anti-FLAG and anti-P-Rex1 antibodies, as indicated below the different panels. Bound: proteins retained in the beads; Cell Extract: 30 μg of protein were loaded for the total fraction. B) CFP-Laforin pull-downs P-Rex1. HEK293 cells were co-transfected with the indicated combination of plasmids expressing Myc-P-Rex1, FLAG-Malin, CFP (empty),

and CFP-Laforin. Extracts were analyzed as in A). A) and B) are representative blots of three independent experiments.

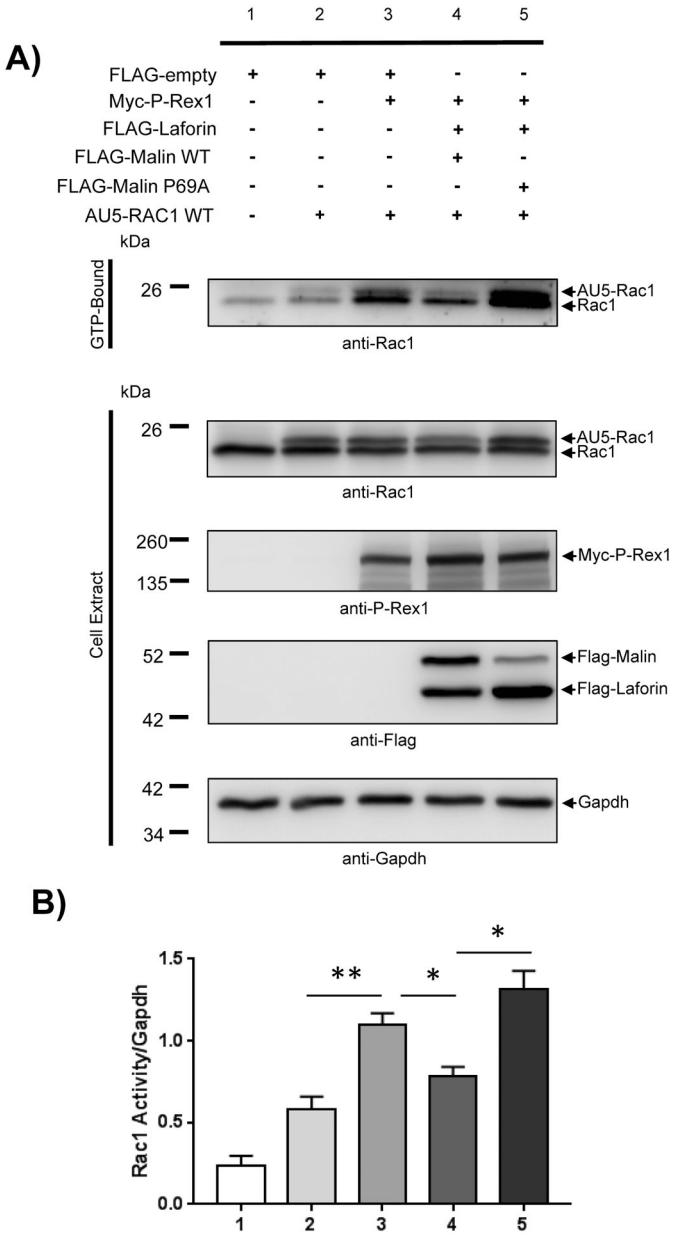

Fig. 5: Malin regulates Rac1 GTPase activity via P-Rex1.

A) Rac1 pulldown assay was performed using a GST fusion protein containing the Rac1 binding domain of PAK1 (GST-RBD-PAK1). HEK293 cells were co-transfected with the plasmids expressing Myc-P-Rex1, FLAG-Laforin, FLAG-Malin, FLAG-Malin P69A, and AU5-Rac1 WT. Cells were lysed and 1.5 mg of protein were incubated with preloaded GST-RBD-PAK1-GSH-beads. The purified bound fraction and 30 μg of the crude extracts were analyzed by Western blot using the indicated antibodies. A representative blot of three independent experiments is shown. B) Quantification of the activated Rac1 signal related to the levels of Gapdh. Values are the mean +/− SEM of three independent experiments (*$p<0.05$, **$p<0.01$).

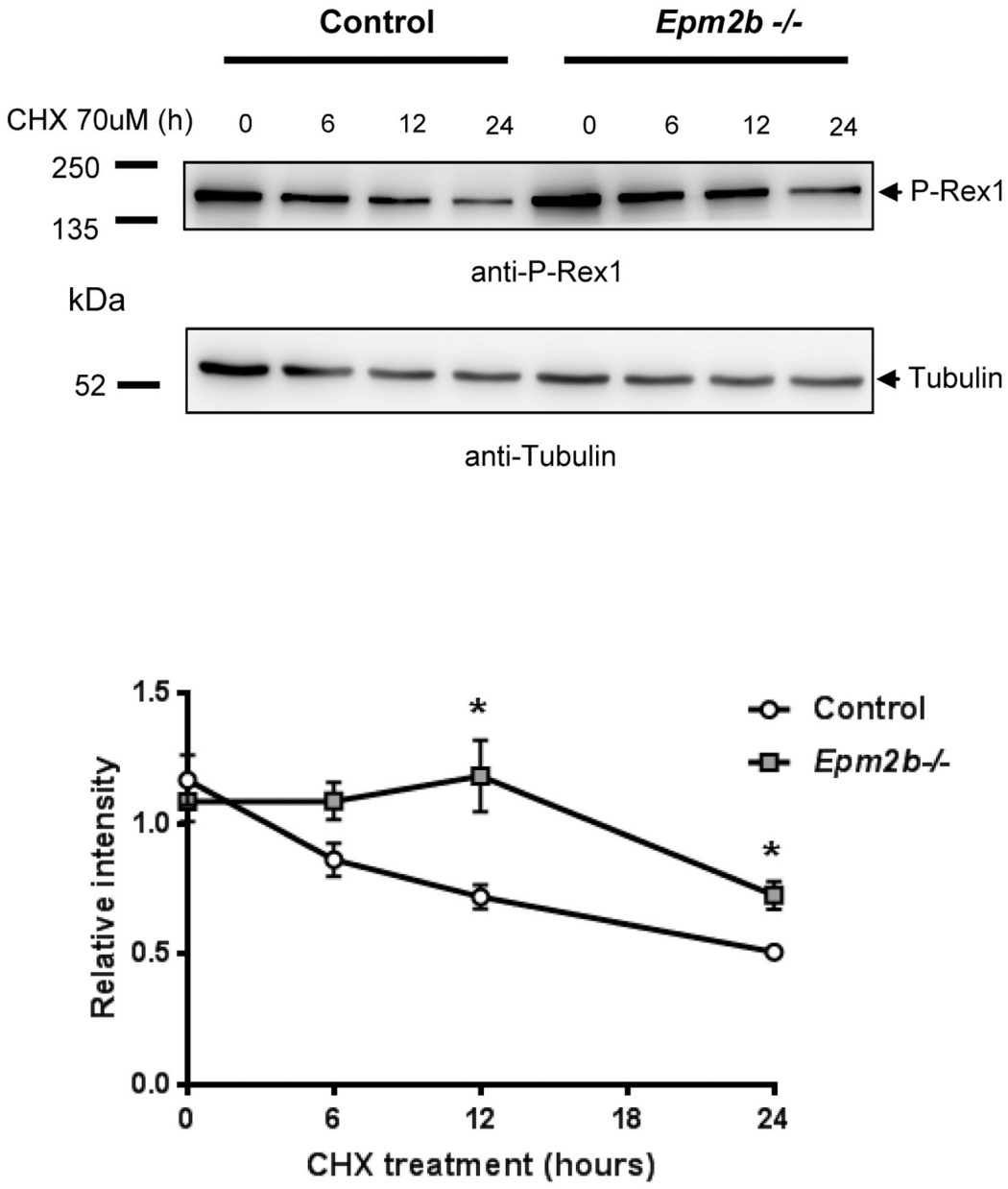

Fig. 6: Analysis of the Degradation Rate of P-Rex1.

Primary astrocytes from control and *Epm2b*−/− mice were treated with 70 μM cycloheximide for different time points (from 0 to 24 h). Cells were lysed and 30 μg of the crude extracts were analyzed by Western blot. At the time points of 12 and 24 h, in *Epm2b*−/− astrocytes the amount of P-Rex1 was higher compared to the control, suggesting impairment in the rate of the degradation process due to the absence of Malin. A representative blot of five independent experiments is shown. In the lower panel, we show the quantification of the relative levels of P-Rex1 to tubulin at each time point. Values are the mean +/− SEM of five independent experiments (*$p<0.05$).

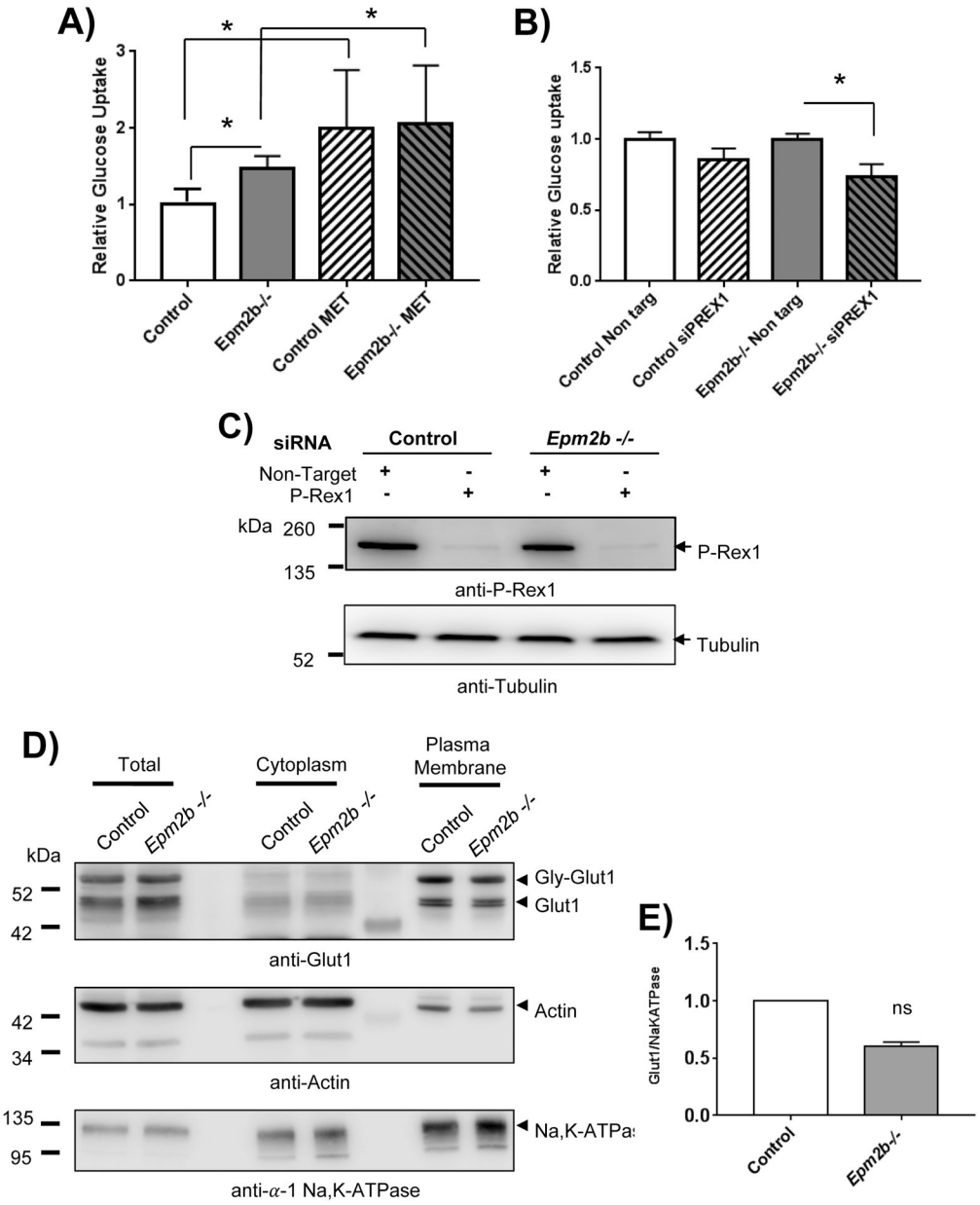

Fig. 7: Glucose uptake and analysis of cell surface proteins by biotinylation.

A) Primary astrocytes (Control and *Epm2b−/−*) were used to measure the rate of glucose uptake as indicated in Materials and Methods. To minimize differences between different samples, we performed the experiment by platting control and *Epm2b−/−* cells at the same time. Then we analyze the glucose uptake and plotted the relative values of glucose transport related to those found in the control sample, which was adjusted to 1. Astrocytes were also treated with 2 mM Metformin for 24 hours, as a control for an increase in glucose uptake. Values are the mean of four independent experiments +/− SEM (*p<0.05). B) The expression of P-Rex1 was silenced in primary astrocytes (Control and *Epm2b−/−*) by using 20 nM of SmartPool P-Rex1 siRNA or Non-Target siRNA (see Materials and Methods). Then, glucose uptake was measured as above. Values are referred to the corresponding

control and *Epm2b*−/− cells treated with Non-Target siRNA, which was adjusted to 1 in each case. Values are the mean of three independent experiments +/− SEM (*p<0.05). C) An aliquot of the treated siRNA cells (30 μg of crude extracts) was analyzed by western blot using anti-P-Rex1 and anti-tubulin (loading control) antibodies. Molecular size markers are indicated on the left. D) Analysis of the cell surface biotinylation assay performed as indicated in Materials and Methods. An aliquot of the lysate was saved for Western blotting (Total fraction). The biotinylated fraction was isolated with NeutrAvidin beads, eluted by the sample buffer containing DTT, and subjected to Western blot analysis (Plasma membrane fraction). The unbound fraction (Cytoplasm) was analyzed too. No differences were observed in the levels of the glycosylated (55 kDa; Gly-Glut1) or the non-glycosylated (45 kDa; Glut1) forms of GLUT1 either in the total fraction or in the plasma membrane fraction. Actin and Na+/K+-ATPase were used as controls of cytoplasm and plasma membrane fractions, respectively. Blots are representative images of three independent experiments. E) Quantification of the levels of GLUT1 related to the levels of Na+/K+-ATPase at the plasma membrane fraction. Values are the mean +/− SEM of three independent experiments; ns: no statistically significant differences.

Table 1:

Differentially ubiquitinated proteins in cells expressing Malin-WT vs Malin-P69A with a fold change >4 and a p-value<0.05. The gene names, the molecular weight, the fold change, the p-value, the number of identified peptides supporting the ubiquitination, and the protein names are indicated.

Gene names	MW (kDa)	Fold Change (WT/P69A)	p-value	Peptides (unique)	Protein names
PREX1	175.9	18.48	0.00181	3	Phosphatidylinositol-3,4,5-trisphosphate-dependent Rac exchanger 1 protein (P-Rex1)
SEH1L	39.6	9.70	0.00027	3	Nucleoporin SEH1L
HSPA4	94.3	8.59	0.00008	43	Heat shock 70 kDa protein 4
SCLT1	80.9	8.23	0.00004	6	Sodium channel and clathrin linker 1
YTHDF2	62.3	8.19	0.01791	7	YTH domain-containing family protein 2
FKBP5	51.2	7.80	0.03059	10	Peptidyl-prolyl cis-trans isomerase FKBP5
HSPA1L	70.4	7.11	0.04710	23	Heat shock 70 kDa protein 1-like
GLMN	68.2	6.89	0.00446	16	Glomulin
KLC2	68.9	6.14	0.01467	7	Kinesin light chain 2
LIN7C	21.8	5.93	0.01001	2	Protein lin-7 homolog C
ANKRD16	39.3	5.40	0.01252	5	Ankyrin repeat domain-containing protein 16
HSP90AB4P	58.3	5.35	0.00031	9	Putative heat shock protein HSP 90-beta 4
HSPH1	92.1	5.11	0.00011	40	Heat shock protein 105 kDa
HSPA4L	94.5	4.66	0.00007	27	Heat shock 70 kDa protein 4L
RCL1	40.8	4.65	0.04792	4	RNA 3-terminal phosphate cyclase-like protein
DLST	48.8	4.63	0.00064	2	Dihydrolipoyllysine-residue succinyltransferase component of 2-oxoglutarate dehydrogenase complex. mitochondrial
STIP1	62.6	4.42	0.00016	25	Stress-induced-phosphoprotein 1
DUSP1	39.3	4.14	0.00033	9	Dual specificity protein phosphatase 1
MKS1	63.3	4.02	0.00443	2	Meckel syndrome type 1 protein
TGFBRAP1	97.2	4.01	0.00582	5	Transforming growth factor-beta receptor-associated protein 1